HELSINKI UNIVERSITY OF TECHNOLOGY
Department of Chemical Technology

Antti J. Niskanen

LIQUID PHASE DEPOSITION OF SILICON DIOXIDE THIN FILMS

Thesis for the degree of Master of Science in Technology.

Espoo, 19 February 2002

Supervisor:

Professor Lauri Niinistö

Instructor:

Sami Franssila, Ph.D.

Preface

This thesis was prepared at the Electron Physics Laboratory of Helsinki University of Technology between February 2001 and February 2002. Much work was also done in the year 2000, at the beginning of which I was—very much by coincidence—sidetracked from my work on porous silicon to the subject of liquid phase deposition.

And this is where that happy coincidence finally led to. Along the way I was delighted by the opportunity to attend my first ever international conference, the Micro and Nano Engineering 2000 held in Jena, Germany. Liquid phase deposition (more specifically, image reversal by that method) was also the subject of my poster presentation there.

I would like to thank Professor Lauri Niinistö for proofreading the manuscript and for his valuable suggestions regarding it. Thanks also to my brother Sampo for the same. But most of all I want to thank the staff of the Electron Physics Laboratory and the Microelectronics Center, especially Dr. Sami Franssila, for their help and encouragement throughout the writing of this thesis.

Espoo, 19 February 2002

Antti J. Niskanen

TEKNILLINEN KORKEAKOULU — DIPLOMITYÖN TIIVISTELMÄ

Kemian tekniikan osasto

Tekijä	Päiväys
Antti J. Niskanen	19. 2. 2002
	Sivumäärä: vii + 56
Työn nimi: Piidioksidiohutkalvojen kasvatus nestefaasimenetelmällä	
Professuuri: Epäorgaaninen kemia	Koodi: Kem-35
Työn valvoja: Professori Lauri Niinistö	
Työn ohjaaja: FT Sami Franssila	

Tässä diplomityössä tutkittiin piidioksidiohutkalvojen kasvatusta nestefaasista (liquid phase deposition, LPD). Kyseessä on matalan lämpötilan prosessi, jossa piidioksidia kasvaa heksafluoropiihappo- (H_2SiF_6) pohjaisesta liuoksesta. Työssä tutkittiin piidioksidin kasvua piin, metallien ja muiden puolijohdeprosessoinnissa käytettävien materiaalien pinnalle sekä kasvunopeuden riippuvuutta kasvatusliuoksen koostumuksesta, lämpötilasta ja valmistusmenetelmästä.

Kasvatettujen kalvojen paksuus ja taitekerroin määritettiin ellipsometrisesti. Kalvon kestävyyttä tutkittiin kemiallisin syövytyskokein ja verrattiin termisesti kasvatettuihin piidioksidiohutkalvoihin. Metalli-oksidi-puolijohde- (metal-oxide-semiconductor, MOS) kondensaattorirakenteista mitattiin kasvatetun oksidin sähköisiä ominaisuuksia.

Työssä esitetään myös kasvunopeuden kannalta kasvatusliuoksen optimaalinen koostumus, jolla kasvatetut kalvot ovat erittäin tasaisia ja niiden taitekerroin poikkeaa vain vähän termisen oksidin taitekertoimesta. Oksidin syöpymisnopeus laimeassa fluorivetyhappoliuoksessa on kuitenkin huomattavasti suurempi kuin termisen oksidin. Paksujen kalvojen kasvatus havaittiin hankalaksi, sillä piidioksidia alkaa saostua kasvatusliuoksessa usean tunnin kasvatuksen jälkeen.

Lopuksi esitetään uudenlainen maskinvalmistusmenetelmä, jolla voidaan tuottaa alle mikrometriluokan rakenteita tavallisesti isompiin rakenteisiin rajoittuvin optisin menetelmin. Menetelmä perustuu valottamalla kuvioidun fotoresistimaskin ohentamiseen happiplasmassa ja näin saadun kuvion kääntämiseen nestefaasikasvatuksen selektiivisyyttä hyödyntäen.

HELSINKI UNIVERSITY OF TECHNOLOGY
Department of Chemical Technology

ABSTRACT OF MASTER'S THESIS

Author	Date
Antti J. Niskanen	19 February 2002
	Pages: vii + 56
Title of thesis	
Liquid phase deposition of silicon dioxide thin films	
Chair	**Chair Code**
Inorganic Chemistry	Kem-35
Supervisor	
Professor Lauri Niinistö	
Instructor	
Sami Franssila, Ph.D.	

This thesis examines the process of liquid phase deposition (LPD) of silicon dioxide, a low-temperature process for depositing silicon dioxide thin films from a hexafluorosilicic acid (H_2SiF_6) based solution. The deposition of silicon dioxide on silicon, metals and other materials used in semiconductor processing is studied, as well as the dependence of the film deposition rate on solution composition, preparation method and temperature.

The thicknesses and refractive indices of deposited films were measured by ellipsometry. The chemical resistance of the film was investigated by etching tests and compared to that of thermally grown silicon dioxide. Metal-oxide-semiconductor (MOS) capacitor structures were fabricated and measured to determine the electrical properties of the oxide.

The composition of the growth solution offering optimal deposition rate is also presented in this work. Films thus grown were found to be extremely uniform and their refractive index differed only slightly from that of thermal oxide. The etch rate of the deposited oxide is, however, significantly greater than that of thermal oxide. The deposition of thick oxide layers was found to be difficult, since silicon dioxide begins to precipitate in the growth solution after several hours of deposition.

Finally, a novel mask-formation technique for deep sub-micron scale dark-field structures (trenches and holes) is demonstrated, utilizing the selective nature of liquid phase deposition. Light-field photoresist patterns (lines and dots) smaller than what is possible by conventional optical lithography alone are fabricated by etching in oxygen plasma. The image is then reversed by selective liquid phase deposition of silicon dioxide.

List of abbreviations

Abbreviation	**Meaning**
a-Si	Amorphous silicon
BHF	Buffered HF (SiO_2-etch solution)
CMOS	Complementary metal-oxide-semiconductor
CVD	Chemical vapor deposition
DC	Direct current
DI	De-ionized (water)
EBL	Electron beam lithography
ECR	Electron cyclotron resonance
HF	Hydrofluoric acid
IR	Infrared
LCD	Liquid crystal display
LDD	Lightly doped drain
LPCVD	Low pressure chemical vapor deposition
LPD	Liquid phase deposition
MOS	Metal-oxide-semiconductor
PECVD	Plasma enhanced chemical vapor deposition
PMMA	Polymethyl methacrylate
RF	Radio frequency
RIE	Reactive ion etching
sccm	Standard cubic cm per minute
SEM	Scanning electron microscopy
TEOS	Tetraethoxysilane
TFT	Thin film transistor
TD-LPD	Temperature-difference based liquid phase deposition
UV	Ultraviolet
XPS	X-ray photoelectron spectroscopy
XRD	X-ray diffraction

Contents

Preface ii

Tiivistelmä iii

Abstract iv

List of abbreviations v

1 Introduction 1

2 Oxide growth on silicon 3
2.1 Native oxide 3
2.2 Thermal oxidation 3
2.3 Plasma oxidation 5
2.4 Chemical vapor deposition 5
2.5 Physical deposition 6

3 Liquid phase deposition 8
3.1 Mechanism 8
3.2 Special features of LPD 11
3.3 Methods 13
3.4 Characterization 14
3.4.1 Growth rate 14
3.4.2 Refractive index 15
3.4.3 Composition 15
3.4.4 Electrical characteristics 16
3.5 Applications 17
3.5.1 Thin film transistors 17
3.5.2 Contact holes 18
3.5.3 CMOS 19
3.5.4 Planarization 20

4 Experimental methods 23
4.1 Materials 23
4.2 Equipment 23
4.3 Deposition procedure 24
4.4 Characterization 25
4.5 MOS capacitor process 26

5 Experimental results **27**
5.1 Growth rate . . . 27
5.1.1 The effect of temperature . . . 27
5.1.2 The effect of boric acid concentration . . . 30
5.1.3 The effect of water addition . . . 31
5.1.4 The effect of the initial H_2SiF_6 concentration . . . 32
5.2 Film characteristics . . . 33
5.2.1 Refractive index and thickness uniformity . . . 33
5.2.2 Etch rate in HF . . . 34
5.2.3 Electrical characteristics . . . 34
5.3 Selectivity of deposition . . . 38
5.4 Maximum thickness of LPD SiO_2 . . . 38

6 Image reversal **40**

7 Conclusions **44**
7.1 Recommended recipe for SiO_2 LPD . . . 44
7.2 Film properties . . . 45
7.3 Selectivity of deposition . . . 46
7.4 Image reversal . . . 46
7.5 Temperature effects . . . 47
7.6 Problems with LPD . . . 47

References **48**

A Additional experimental data **52**

B Oxygen plasma ashing **56**

Chapter 1

Introduction

Modern semiconductor electronics is almost entirely based on silicon. Only a few niche applications use other semiconductor materials, such as gallium arsenide in optoelectronics. It is therefore natural that silicon dioxide has long been the de-facto insulator material in semiconductor devices, as it is easily formed on silicon by simple thermal oxidation. Although high dielectric constant materials are nowadays gaining importance, silicon dioxide remains the most widely used dielectric.

The importance of silicon has seen a fairly recent increase not only as an electronic material, but as a mechanical material as well. In the growing field of micromechanics, mechanical structures such as acceleration sensors, pressure sensors, ink jet nozzle arrays and even complete instruments like gas chromatographs are fabricated in microscopic dimensions [1]. Such devices benefit from the mechanical properties of silicon, including its hardness, high elastic modulus (resistance to deforming under stress) and tensile strength [2]. Moreover, fabricating sensors on silicon offers the possibility of *e.g.* integrating a sensor and its associated electronics on the same chip. But most importantly, silicon micromechanics relies on the extensive knowledge of silicon processing technology which the decades of use in the semiconductor industry has provided. Silicon dioxide finds use in micromechanics not only as an insulator material, but as a structural material and a useful mask material for silicon etching as well.

Out of the basic processes of silicon dioxide formation, each has its strengths and weaknesses. Most of them require expensive process equipment, hazardous gases and high processing temperatures. A relatively recent development is a process called liquid phase deposition (LPD). The method is especially attractive due to its low process temperature, low-cost equipment and easily handled materials. The selective nature of the deposition process may also prove useful in many applications.

This thesis focuses on the growth of silicon dioxide thin films from liquid phase, the properties of the deposited films, and their applications. An overview of the

traditional growth methods of silicon dioxide thin films is given in Chapter 2, followed by a review of published work on the LPD process and applications of LPD oxide in Chapter 3. Methods used for sample preparation and characterization in this work are explained in Chapter 4, and results are presented in Chapter 5. A novel mask-formation technique for submicron features is presented in Chapter 6. The main results are discussed in the final chapter (Chapter 7).

Chapter 2

Oxide growth on silicon

Silicon dioxide can be grown by several methods. On bare silicon substrates, oxide films can be formed by oxidation, in which silicon is consumed as it reacts with oxygen from the surrounding atmosphere. Oxide can also be deposited by either chemical or physical means, independently of the substrate composition.

After the issue of oxidation versus deposition, the process temperature is the next major factor in the comparison of various SiO_2 processes. Lower temperatures are desirable to reduce dopant diffusion, interdiffusion of films, and defect generation in silicon. On the other hand, high temperatures (above 450°C) are not permissible when dealing with soda lime glass substrates *e.g.* in the fabrication of thin film transistors for liquid crystal displays. [3]

2.1 Native oxide

Absolutely the simplest method for oxide formation must be simply waiting for a native oxide to form on a silicon wafer. After surface oxide has been stripped with HF, a new oxide layer of typically ∼1.5 nm will form within a few hours [4, pp. 293–294]. A native (or "chemical") oxide will also easily form during wet processing *e.g.* standard RCA cleaning [4, p. 433].

Native oxide is usually of very poor quality and contains a whole spectrum of impurities picked up from the processing and storage ambient. It is certainly not sufficient for any application where oxide films are required, and is therefore mostly a nuisance when processing on a bare silicon surface.

2.2 Thermal oxidation

The simplest practical method of forming silicon dioxide on a silicon wafer is by thermal oxidation. Oxidation is carried out at high temperatures, usually

between 850°C and 1100°C. Silicon can be oxidized in a dry oxygen atmosphere (dry oxidation):

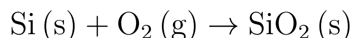

$$\mathrm{Si\,(s) + O_2\,(g) \rightarrow SiO_2\,(s)}$$

or in an atmosphere containing water vapor (wet oxidation):

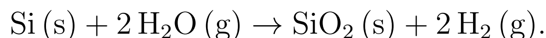

$$\mathrm{Si\,(s) + 2\,H_2O\,(g) \rightarrow SiO_2\,(s) + 2\,H_2\,(g).}$$

SiO_2 formation takes place at the Si/SiO_2 interface, thus, the oxygen or water molecules must diffuse through the oxide layer in order to react with the silicon. Due to its smaller size, a H_2O molecule can diffuse through the oxide faster than O_2, which makes wet oxidation faster than dry oxidation [5, p. 71]. Silicon in turn is consumed in the reaction, about 0.44 µm for each µm of oxide produced [6, p. 293].

Thermal oxidation is quite accurately described by the Deal-Grove model [5, pp. 68–74], which takes on the following form for thin oxides:

$$t_{\mathrm{ox}} \approx \frac{B}{A}(t+\tau) \tag{2.1}$$

but the following for thicker oxides:

$$t_{\mathrm{ox}} \approx \sqrt{B(t+\tau)} \tag{2.2}$$

where A and B are tabulated values and τ is calculated from the initial oxide thickness at the beginning of the oxidation process. Initially, the oxide thickness t_{ox} increases linearly with time t (equation 2.1), but above 100 nm oxidation becomes diffusion controlled, the rate law becomes parabolic (equation 2.2), and the growth rate decreases rapidly.

The oxidation rate of silicon is very low—only about 60 nm of SiO_2 is formed during the first hour of dry oxidation at 1000°C [6, p. 293]. Thus, the thickness of thermal oxides can be controlled very accurately, but films thicker than 1 µm are impractical to achieve even by wet oxidation.

Thermal oxidation has some problems due to the fact that it is literally an *oxidation* process, not an oxide *deposition* process. Due to the volume change associated with the oxidation of silicon, enormous stresses can develop at the Si/SiO_2 interface. However, viscous flow of the oxide relieves this stress when oxidation is performed above 950°C. The behaviour of dopant atoms must also be considered in thermal oxidation. Due to the differences in dopant solubilities in silicon and oxide, dopant atoms can preferentially segregate either into the silicon or into the oxide layer. This causes a sharp increase (*e.g.* in the case of boron) or decrease (*e.g.* phosphorous or arsenic) in the silicon doping level near the Si/SiO_2 interface. [6, pp. 296–300]

Due to its high process temperature, thermal oxidation is incompatible with polymers, most metals used in the semiconductor industry, and substrates with a low melting point *e.g.* soda lime glass. It also increases dopant diffusion in electronic devices. However, thermally grown oxide contains the fewest defects

in the bulk and at the SiO_2/Si interface [5, p. 68], and is therefore generally considered the de-facto standard in comparison with other SiO_2 growth and deposition processes.

2.3 Plasma oxidation

Plasma oxidation is performed at a lower pressure than thermal oxidation and, more importantly, at a lower temperature. The reactive ions, electrons, radicals and radiation produced by the plasma enhance the oxidation reaction. Thus, growth rates near and even above those of thermal oxidation are possible at temperatures less than 600°C, where practically no thermal oxidation would take place.

The plasma can be generated by microwave, RF or ECR excitation, and either O_2 or N_2O can be used as the oxidant. When the potential of the silicon substrate is left floating, the process is referred to as plasma oxidation. Even higher growth rates can be achieved by a process called *anodization*, where a positive bias is applied to the substrate to enhance the transport of negatively charged species. Hess [3] has reported an 85 nm/h oxidation rate at 600°C by plasma anodization—greater than the 60 nm/h by dry oxidation at 1000°C mentioned earlier.

The growth rate of SiO_2 in plasma oxidation is even higher for amorphous silicon (*a*-Si) than for crystalline silicon. Even at temperatures low enough to be compatible with photoresist, about 3 nm of oxide is formed within seconds, after which the oxidation rate falls rapidly. ECR plasma oxidation of *a*-Si has been used by Kurihara *et al.* [7] for the reversal of EBL-patterned photoresist films (see Chapter 6).

2.4 Chemical vapor deposition

Chemical vapor deposition (CVD) is a versatile method for depositing thin films from gaseous precursors. A variety of metallic, semimetallic, oxide, carbide and nitride films can be deposited from suitable volatile precursors, usually hydrides, halides or volatile organic or metallo-organic compounds. The gaseous precursors react to form the deposited film, rather than consuming surface material from the substrate as oxidation does. Deposition is therefore possible regardless of the substrate composition. The reactions proceed on the surface of the heated substrate, and can roughly be classified as follows: [8, pp. 51–57]

Thermal decomposition (pyrolysis):

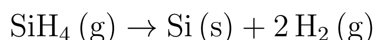

$$SiH_4\,(g) \rightarrow Si\,(s) + 2\,H_2\,(g)$$

Reduction (*e.g.* by hydrogen):

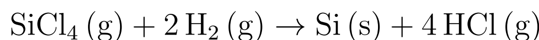

$$SiCl_4\,(g) + 2\,H_2\,(g) \rightarrow Si\,(s) + 4\,HCl\,(g)$$

Oxidation or hydrolysis:

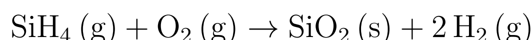

$$SiH_4\,(g) + O_2\,(g) \rightarrow SiO_2\,(s) + 2\,H_2\,(g)$$

Other (*e.g.* nitridation):

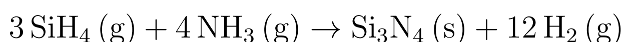

$$3\,SiH_4\,(g) + 4\,NH_3\,(g) \rightarrow Si_3N_4\,(s) + 12\,H_2\,(g)$$

Ordinary thermal CVD, also referred to as low pressure CVD or LPCVD, is activated by the hot surface of the substrate and requires high temperatures, typically 600–900°C. The deposition pressure is usually on the order of one Torr (∼100 Pa), but can vary in a wide range, from atmospheric pressure down to milliTorrs (∼0.1 Pa). At higher pressures an inert diluent gas must be used to prevent gas-phase nucleation. [5, pp. 323–329]

The CVD process can be enhanced by activating the gaseous precursors by means of a plasma generated with a radio-frequency electric field. For example, SiH_4 produces free radicals SiH, SiH_2 and SiH_3, which easily react with the substrate surface [9, p. 119]. The plasma enhanced CVD (PECVD) method therefore allows substrate temperatures to be considerably lower, typically around 300–400°C. While the lower process temperature is the major advantage of PECVD, it can lead to incomplete desorption of reaction byproducts and to non-stoichiometric films. The latter can however also be an advantage, as it allows fine-tuning of the film's properties for specific applications [8, p. 103].

Silicon dioxide can be grown by CVD from silane (SiH_4) and either oxygen or nitrous oxide (N_2O). Deposition temperatures of 1000°C (LPCVD) and 300°C (PECVD) are typical. Tetraethoxysilane (TEOS, $(C_2H_5O)_4Si$), a stable liquid, is another widely used silicon precursor for CVD. It has obvious advantages from the safety point of view, but requires higher deposition temperatures than silane. [5, pp. 328–331]

2.5 Physical deposition

Physical deposition comprises various methods such as thermal or e-beam evaporation, laser ablation and sputtering. In the first three, material is evaporated by heating, either in bulk with an electrically heated filament, or locally by the action of an electron beam or laser. In the sputtering process, ions from

an argon plasma are accelerated towards a target made of the material to be deposited. The ion bombardment causes target atoms and molecules to be ejected or *sputtered* from the target surface. This material condenses to form a film on the substrate surface.

Physical deposition methods are commonly used for metalization of integrated circuits. Silicon dioxide can also be deposited by e-beam evaporation [10], though the method is not very common. Sputtering of insulating targets such as SiO_2 is possible if an RF discharge is used instead of the more common DC glow discharge [5, p. 293]. Sputtering is an even lower temperature process than PECVD—usually it is performed at room temperature. But while sputtering is the most commonly used metal deposition process, sputtering of SiO_2 is very rarely even mentioned in literature.

Chapter 3

Liquid phase deposition

"High-silica fluosilicic acids", *i.e.* aqueous silica-containing solutions of hexafluorosilicic acid H_2SiF_6 have been extensively studied by Thomsen [11]. It turns out that their silica content can be much larger (by up to 18%) than expected from the formula H_2SiF_6. This point should be emphasized: Even though H_2SiF_6 is often considered the product of SiO_2 dissolving in HF, it readily dissolves more SiO_2 (and therefore etches glass as well) to form a saturated solution corresponding quite closely in stoichiometry to $H_2[SiF_6 \cdot SiF_4]$. H_2SiF_6 solutions containing various amounts of dissolved silica have been used to form anti-reflection coatings on glass surfaces by etching a porous layer on the surface, either in the vapor phase [12] or liquid phase [13].

Interestingly enough, the very same solutions were later to become the basis for *deposition* of silicon dioxide films. The liquid phase deposition (LPD) process was first reported in 1988 by Nagayama *et al.* [14], who deposited SiO_2 films on soda lime glass by immersion in supersaturated H_2SiF_6 solution. The method has since undergone extensive study by several research groups due to its attractive features *e.g.* low cost, low thermal budget and selectivity.

3.1 Mechanism

SiO_2 LPD can be considered the reverse of SiO_2 dissolving in hydrofluoric acid. As presented in [14], the reaction

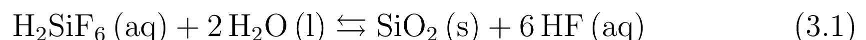

$$H_2SiF_6\,(aq) + 2\,H_2O\,(l) \leftrightarrows SiO_2\,(s) + 6\,HF\,(aq) \tag{3.1}$$

is an equilibrium reaction, which is shifted to the right according to Le Châtelier's principle by the addition of water or by the removal of HF. The latter is accomplished by adding a HF-scavenger, such as boric acid [14] or aluminum [15], which form stable complexes with fluoride ions:

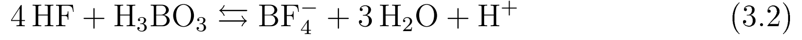

$$4\,\mathrm{HF} + \mathrm{H_3BO_3} \leftrightarrows \mathrm{BF_4^-} + 3\,\mathrm{H_2O} + \mathrm{H^+} \tag{3.2}$$

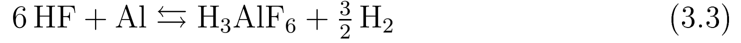

$$6\,\mathrm{HF} + \mathrm{Al} \leftrightarrows \mathrm{H_3AlF_6} + \tfrac{3}{2}\,\mathrm{H_2} \tag{3.3}$$

Either way, a "supersaturated" solution results, *i.e.* a solution containing too much SiO_2, and therefore capable of deposition. Deposition of SiO_2 begins as soon as a suitable substrate is immersed.

It is noteworthy that water acts not only as a solvent in the reaction, but also as a reagent. Thus, in a SiO_2-saturated solution, reaction 3.1 can be made to proceed with the addition of water only [16, 17], without any HF-scavengers. While many articles refer to the addition of water as "dilution" of the H_2SiF_6 solution, it should rather be regarded as addition of a reagent causing a change in the total volume of the reagent solution.

Since the dissolution of SiO_2 in HF is an exothermic reaction [11], heating the growth solution is expected to enhance deposition. In fact, Yeh *et al.* [18] have demonstrated temperature-dependent LPD (TD-LPD), based only on a change in temperature with no addition of water or H_3BO_3.

The actual mechanism in SiO_2 LPD is believed to involve intermediate species formed by the hydration of H_2SiF_6 or saturation of the HF-containing solution with silicic acid [19, 20, 21]:

$$\mathrm{H_2SiF_6} + (4-m)\,\mathrm{H_2O} \leftrightarrows \mathrm{SiF}_m(\mathrm{OH})_{4-m} + (6-m)\,\mathrm{HF} \tag{3.4}$$

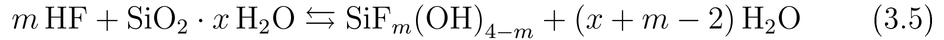

$$m\,\mathrm{HF} + \mathrm{SiO_2}\cdot x\,\mathrm{H_2O} \leftrightarrows \mathrm{SiF}_m(\mathrm{OH})_{4-m} + (x+m-2)\,\mathrm{H_2O} \tag{3.5}$$

Yeh *et al.* [17], on the other hand, propose SiF_4 as a necessary intermediate species. According to them, saturation of the H_2SiF_6 solution with SiO_2 causes the following reaction to occur:

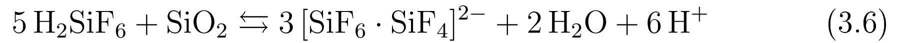

$$5\,\mathrm{H_2SiF_6} + \mathrm{SiO_2} \leftrightarrows 3\,[\mathrm{SiF_6}\cdot\mathrm{SiF_4}]^{2-} + 2\,\mathrm{H_2O} + 6\,\mathrm{H^+} \tag{3.6}$$

As the nucleophile H_2O attacks the weak Si−F−Si bond (Fig. 3.1), SiF_4 is formed:

$$[\mathrm{SiF_6}\cdot\mathrm{SiF_4}]^{2-} + 2\,\mathrm{H_2O} \leftrightarrows \mathrm{SiF_4(OH)_2^{2-}} + \mathrm{SiF_4} + 2\,\mathrm{HF} \tag{3.7}$$

Further, $SiF_4(OH)_2^{2-}$ will react to form more SiF_4:

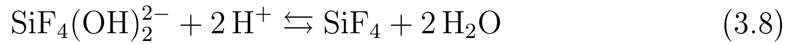

$$\mathrm{SiF_4(OH)_2^{2-}} + 2\,\mathrm{H^+} \leftrightarrows \mathrm{SiF_4} + 2\,\mathrm{H_2O} \tag{3.8}$$

The silicic monomer $Si(OH)_4$ is then formed by the hydrolysis of SiF_4:

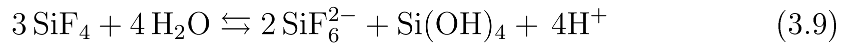

$$3\,\mathrm{SiF_4} + 4\,\mathrm{H_2O} \leftrightarrows 2\,\mathrm{SiF_6^{2-}} + \mathrm{Si(OH)_4} + 4\mathrm{H^+} \tag{3.9}$$

Since deposition occurs only on the surface of the substrate (*i.e.* SiO_2 particles do not begin to form in the solution), it seems that the surface lowers the activation barrier of the reaction. Chou and Lee [19] propose that the fluorinated

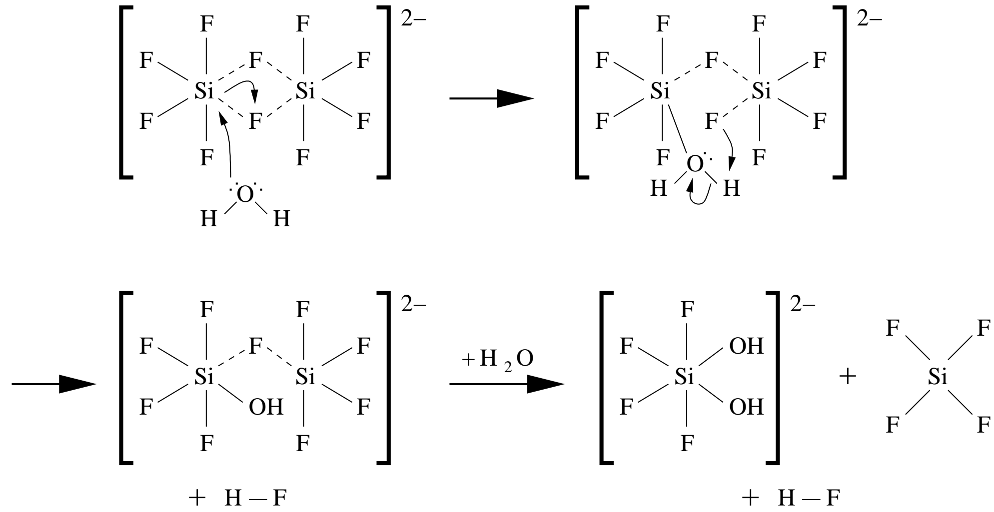

Figure 3.1: The $[SiF_6 \cdot SiF_4]^{2-}$ complex and its reaction with water [17]

silicic acid monomers formed in 3.4, 3.5 or 3.9 react with fluorine or hydroxyl groups in the substrate surface to form new Si–O bonds and HF:

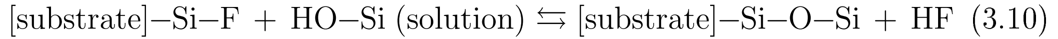

$$\text{[substrate]–Si–F} + \text{HO–Si (solution)} \leftrightarrows \text{[substrate]–Si–O–Si} + \text{HF} \quad (3.10)$$

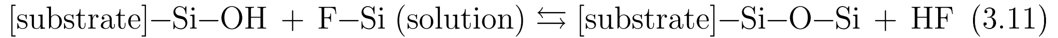

$$\text{[substrate]–Si–OH} + \text{F–Si (solution)} \leftrightarrows \text{[substrate]–Si–O–Si} + \text{HF} \quad (3.11)$$

Other mechanisms have been proposed as well [17, 20, 21], where siloxane oligomers, or polysilicic acid, are formed (for clarity, fluorine atoms are ignored):

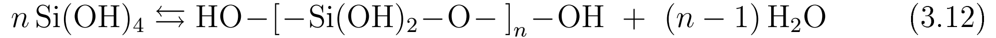

$$n\,\text{Si(OH)}_4 \leftrightarrows \text{HO}-[-\text{Si(OH)}_2-\text{O}-]_n-\text{OH} + (n-1)\,\text{H}_2\text{O} \quad (3.12)$$

Due to their low concentration in the growth solution, the oligomers do not react with each other, which would lead to liquid phase nucleation and precipitation in the solution. Rather, they adsorb onto the substrate surface, and together with surface hydroxyl groups undergo acid catalyzed dehydration to form new Si–O bonds:

$$\text{[substrate]}-\text{Si}-\text{OH} + \text{HO}-\text{Si (solution)} \leftrightarrows \text{[substrate]}-\text{Si}-\text{O}-\text{Si} + \text{H}_2\text{O} \quad (3.13)$$

In either case, the substrate surface structure is critical for the onset of deposition. According to Chou and Lee [19], the behaviour of a silicon surface in a HF-based solution is dominated by the following equilibria:

$$\text{[substrate]}-\text{Si}-\text{H} + \text{H}_2\text{O} \leftrightarrows \text{[substrate]}-\text{Si}-\text{OH} + \text{H}_2 \quad (3.14)$$

$$\text{[substrate]}-\text{Si}-\text{OH} + \text{HF} \leftrightarrows \text{[substrate]}-\text{Si}-\text{F} + \text{H}_2\text{O} \quad (3.15)$$

$$\text{[substrate]}-\text{Si}-\text{F} + \text{HF} \leftrightarrows \text{[substrate]}-\text{Si}-\text{H} + \text{H}_2\text{SiF}_6 \quad (3.16)$$

If the HF-concentration is below a critical level, a hydrogen terminated surface will be converted by the action of water to a hydroxyl terminated one (3.14). If, however, the HF-concentration is too high, conversion of existing hydroxyls (3.15) will dominate, and any oxide film present will be etched. Since LPD will occur on a hydroxyl terminated surface only, growth will begin on a HF-treated surface only after sufficient reoxidation by water, resulting in delayed growth. On surfaces without hydroxyl groups, such as metals and organics (including photoresist), LPD should not occur at all.

Surface hydrophobicity has been studied by Homma *et al.* [20] as an alternative cause for the observed selectivity of LPD. However, no conclusive relationship between the two has been found.

3.2 Special features of LPD

Conventional methods of oxide deposition and growth require expensive equipment involving high temperatures and possibly requiring vacuum systems. Explosive and toxic gases such as hydrogen and silane are also involved, requiring extensive safety measures. LPD on the other hand is a very simple process which works at atmospheric pressure and effectively room temperature, and requires only inexpensive equipment (*i.e.* a magnetic stirrer-hotplate and a filtration system). Also the chemicals involved are relatively safe, and easily handled in liquid form.

The low process temperature of LPD is one of its major strengths not only from the equipment point of view. It is ideal when materials previously deposited on the substrate are incompatible with high temperature processing. Aluminum, for example, would melt in thermal oxidation, whereas polymer layers *e.g.* photoresist may melt or decompose even at the $\sim$300°C temperature commonly used in PECVD. Soda lime glass substrates may also rule out high-temperature processing. An additional advantage in replacing high-temperature oxidation and deposition with a room temperature process is the decreased overall thermal budget, thus reducing dopant diffusion in electronic devices.

The second major advantage of LPD is the selectivity of deposition, *i.e.* SiO_2 is deposited on some materials but not on others (Fig. 3.2). This enables many processes to be simplified or improved from their more conventional processing approaches (Section 3.5). As mentioned in Section 3.1, LPD is believed to occur only on hydroxyl-terminated surfaces, and should therefore be selective to *e.g.* photoresist, silicon nitride and metals. Selectivity to photoresist is widely reported, *e.g.* [22, 23, 24]. Homma *et al.* [20] report on the selectivity to tungsten, whereas deposition is observed on sputtered WSi_x, probably due to a native SiO_2 layer on its surface. Selectivity to Si_3N_4 is also reported by several investigators [21, 25, 26]. A bare silicon surface, stripped of its native oxide layer with HF, exhibits very little [19] or no deposition [20].

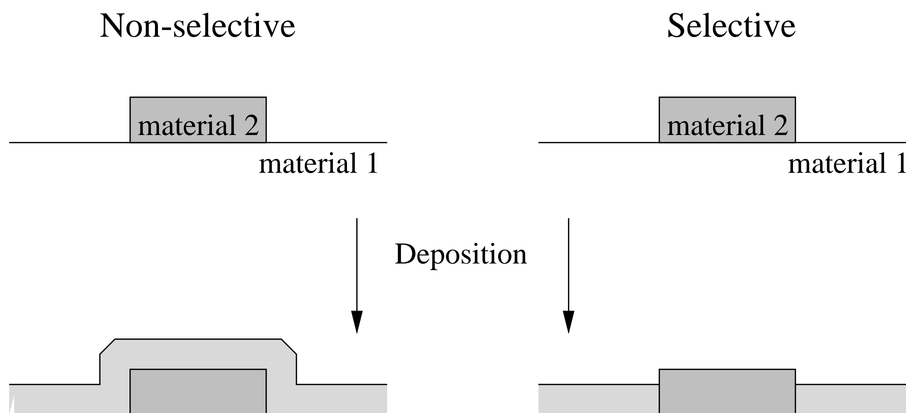

Figure 3.2: Selective versus non-selective deposition

As can be expected, LPD is conformal, *i.e.* deposition occurs on vertical sidewalls of structures identically to horizontal surfaces (Fig. 3.3). Lee *et al.* [26] have investigated the use of SiO_2 LPD for trench filling and several research groups have utilized it for planarization (Section 3.5.4) [20, 27].

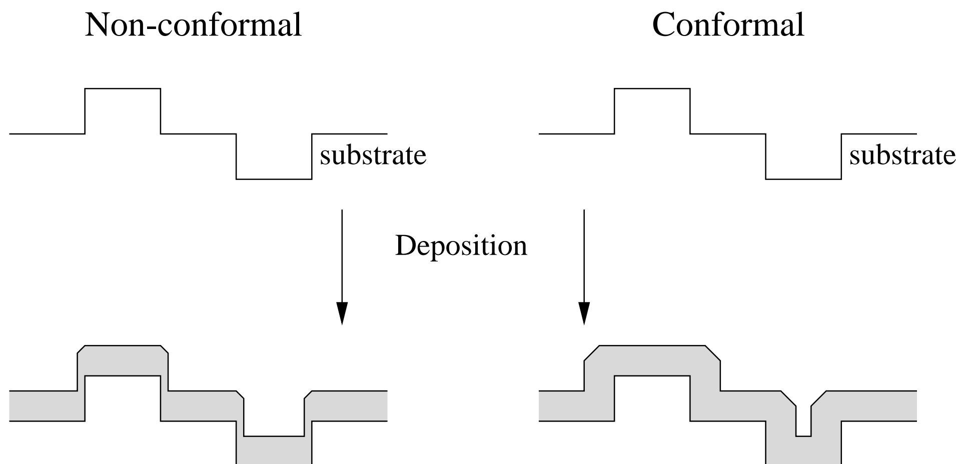

Figure 3.3: Conformal versus non-conformal deposition

In addition to silicon and glass substrates, SiO_2 LPD is also possible on gallium arsenide and indium phosphide substrates. Pretreatment of the GaAs substrate with ammonium hydroxide solution near room temperature has been found to enrich the surface hydroxyl concentration and thus promote LPD [28], whereas InP requires no special pretreatment [29]. Plastic substrates (polycarbonate and PMMA) can be successfully coated with LPD SiO_2 by first treating them with a silane coupling agent (γ-aminopropyltriethoxysilane or N-β-(aminoethyl)-γ-aminopropyltrimethoxysilane for polycarbonate substrates, γ-methacryloxypropyltrimethoxysilane for PMMA substrates) and then with the hydrolysis product of TEOS, before deposition [30].

3.3 Methods

The original process of Nagayama *et al.* [14] is as follows:

1. Dilute 4 mol/dm^3 H_2SiF_6 to 2 mol/dm^3
2. Heat solution to 35°C
3. Add SiO_2, stir for 16 hours
4. Filter
5. Add H_3BO_3
6. Immerse substrate

Two variations of the process exist, differing in the order of the process steps. The methods, denoted process A and B by Chou and Lee [19] and route I and II in [31] (the latter convention will be used here) are depicted in Fig. 3.4. In route I, the H_2SiF_6 solution is saturated with SiO_2 prior to dilution with water, whereas in route II the solution is first diluted, then saturated. Since water is a reagent in the reaction, supersaturation may be reached in route II already during dilution of H_2SiF_6. Thus, the added silica powder may actually *deplete* the solution of dissolved SiO_2 by providing an enormous surface area for deposition to occur on. Route II therefore requires a greater amount of H_3BO_3 to achieve the same level of supersaturation as route I. Not surprisingly, route I is the more commonly seen variant in the literature.

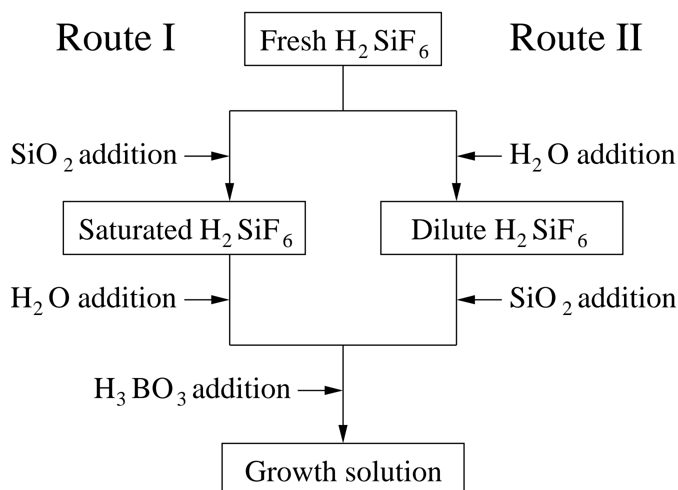

Figure 3.4: Two routes for growth solution preparation

To shorten the time required for saturation of the H_2SiF_6 solution, silicic acid ($SiO_2{\cdot}x\,H_2O$) can be used instead of SiO_2 [32]. Silicic acid contains many hydroxyl groups and is therefore more easily soluble in HF.

Boric acid is by far the most popular HF-scavenger used in the growth solution. While most LPD processes reported in literature add all of the required boric acid prior to immersion of the substrates, Homma *et al.* [20, 33], Horiuchi *et al.* [23] and Yeh *et al.* [34, 35] utilize constant addition of H_3BO_3 solution during deposition with an automatically controlled dripper. Aluminum can also be used to achieve supersaturation [15, 30]. Kitaoka *et al.* [30] used a pump to circulate the growth solution past the substrates and aluminum metal so that aluminum is dissolved during the entire deposition process, analogously to constant addition of H_3BO_3. Other methods of supersaturating the H_2SiF_6 solution are addition of water only [16, 17] and temperature-difference based LPD (TD-LPD) [18]. In TD-LPD, the H_2SiF_6 solution is saturated at a temperature near 0°C, filtered, and heated prior to substrate immersion to create a supersaturated growth solution.

The growth solution is reported to stay clear indefinitely as long as the H_3BO_3 concentration is below a certain level [31], so most investigators simply filter the H_2SiF_6 solution after saturation with SiO_2. Chanthamaly *et al.* [16], on the other hand, achieve high growth rates by constantly circulating the solution through a microfilter to remove any SiO_2 particles that form during deposition.

3.4 Characterization

3.4.1 Growth rate

The growth rate of oxide in LPD depends mainly on the composition of the growth solution and the deposition temperature. Since the reaction is surface controlled, the volume of the growth solution and the surface area of the substrate have no effect on the deposition rate. Results by many investigators are summarized in a review by Chang *et al.* [31]. Growth rates range from a few nanometers per hour to over 250 nm/h reported by Chou and Lee [19]. All publications agree that the deposition rate increases with increasing temperature and H_3BO_3 concentration. There is, however, significant variation in the deposition rates reported by different investigators, even at equal boric acid concentrations. In some cases the difference is explained by the choice of growth solution preparation route. In other cases the H_2SiF_6 saturation time and temperature, or the choice of silicon dioxide or silicic acid in the saturation step may cause differences in the initial state of the growth solution.

The exposed surface area of the solution and the associated evaporation losses may be yet another factor affecting the reagent concentrations in the growth solution. Formation of powdery SiO_2 has been observed above the liquid surface at higher deposition temperatures implying evaporation of more than just water [31], and indeed even at room temperature glass can be etched by the vapors from a solution of H_2SiF_6 [12]. Unfortunately, the exact reaction vessel geometries are seldom reported.

A small enhancement in growth rate by UV illumination has also been reported by Huang *et al.* [36]. The effect becomes slightly more pronounced at higher H_3BO_3 and H_2SiF_6 concentrations. Of the species found in the growth solution, only SiF_6^{2-} exhibits strong absorption of UV radiation, indicating that it may be activated to form intermediate species.

3.4.2 Refractive index

The refractive index of LPD SiO_2 films is typically around 1.43 [31]. At higher boric acid concentrations (*i.e.* higher deposition rates) the refractive index tends to decrease slightly [36]. Post-deposition annealing also causes a slight decrease in the refractive index with increasing annealing temperature, until at about 600°C the refractive index suddenly increases almost to that of thermal oxide ($n = 1.465$ [37]). This behaviour is attributed to the release of water from the oxide, and conversion of $Si-F$ bonds to $Si-O-Si$ bonds at 600°C [17].

3.4.3 Composition

The composition of LPD SiO_2 films has been studied extensively using infrared spectroscopy and x-ray photoelectron spectroscopy (*e.g.* [14, 15, 16, 18, 19]). In general, very strong Si–O–Si stretching peaks are seen in IR-spectra, with Si–F stretching also visible, and very faint OH-stretching. Increasing deposition rate is found to increase the signals from terminating bonds ($-OH$ and $-F$) and decrease the $Si-O-Si$ signal, indicating a more porous structure [18, 19]. Nagayama *et al.* [14] report that LPD SiO_2 contains more Si–O–Si bonds than oxide films deposited by other means (CVD, vacuum evaporation and dipping method) indicating higher film quality. According to XRD-measurements the oxide films are amorphous [15].

XPS studies indicate the ratio of Si to O is very close to 1:2 [14, 15]. The fluorine content of LPD SiO_2 films can be up to 4.75 atomic-% prepared by addition of water only [16], and up to 8.9% by temperature-difference based LPD [18]. If ammonium hydroxide is added to the growth solution, ammonia molecules compete with the silicic acid monomers in the reaction with surface hydroxyls, incorporating nitrogen atoms in the film and producing silicon oxynitride [38].

Reportedly, the composition of LPD SiO_2 films is affected very little by the concentration of Na, K and Ca impurities in the growth solution [39]. According to Hishinuma *et al.* [15], the impurity concentration of the film is further reduced by the use of aluminum instead of boric acid in growth solution preparation. Lu and Hwu [40] report that the use of aluminum increases the electric breakdown field of the SiO_2 film and its resistance to radiation damage, due to the incorporation of aluminum atoms in the film.

3.4.4 Electrical characteristics

Table 3.1 presents some of the reported electrical characteristics of LPD SiO_2 films. The dielectric constant ϵ depends on the amount of fluorine incorporated in the film and possible post-deposition annealing steps. The dielectric constant can be significantly lowered from that of thermal oxide (ϵ=3.85 [41, p. 602]) which is useful for reducing the parasitic capacitance in integrated circuits. The breakdown voltages (V_{BD}) are lower than the ~12 MV/cm typical to thermal oxide [5, p. 79], as can be expected for deposited oxides.

Table 3.1: Reported electrical characteristics of LPD SiO_2 films

Property	Values	Reference
ϵ	3.33–3.34	[42]
	3.5	[34, 35]
	3.46–3.56	[18]
	3.0–3.8	[16]
	3.7–3.9	[33]
V_{BD}	6.3–7.2 MV/cm	[33]
	7 MV/cm	[35]
	7–8 MV/cm	[34]
	9 MV/cm	[32]
J_{leak}	4.6 nA/cm^2 *)	[42]
	6.9–390 nA/cm^2 *)	[18]
	3 nA/cm^2 **)	[34]

*) At 2 MV/cm
**) At 4 MV/cm

Table 3.2 presents more detailed leakage current density data by Yeh *et al.* [18] measured from TD-LPD deposited gate oxides. Leakage currents were measured as deposited and after 30 minutes of annealing in nitrogen at 400°C. Annealing appears to degrade the insulating properties of the film, more notably for films deposited at higher temperatures due to their greater number of terminating bonds and subsequent defects created during annealing.

Table 3.2: Leakage current density in TD-LPD deposited SiO_2 [18]

Deposition temp. (°C)	Leakage current density (nA/cm^2)	
	as-deposited	annealed
15	6.9	9.0
25	4.6	23
35	360	2000

3.5 Applications

3.5.1 Thin film transistors

Thin film transistors (TFTs) are used as switching devices in active matrix liquid crystal displays. Formation of the gate insulator in polysilicon TFTs by thermal oxidation degrades the electron mobility, whereas the common low-temperature alternative, PECVD, is a complex process requiring expensive equipment and is especially difficult for large-area devices such as computer displays. Yeh *et al.* [44] have successfully applied LPD to form gate insulators [34, 35, 44] and studied the effects of annealing on the LPD gate insulator.

The low processing temperature of LPD is a major advantage especially when processing on soda lime glass substrates. In large-area microelectronics, such as LCDs, hydrogenated amorphous silicon (a-Si:H) is gaining interest. Silicon nitride is widely used as gate insulator in such devices, but it suffers from high mechanical stress. Silicon dioxide, deposited by conventional low-temperature processes, does not give satisfactory results on a-Si:H due to a high density of interface states. LPD SiO_2 gates, however, were used by Yeh and Lee [45] in inverted staggered a-Si:H TFTs (whose structure is depicted later in Fig. 3.9 as a cross-sectional view. A conventional TFT is depicted in Fig. 3.5.) on glass substrates, and their bulk and interface properties were found to be comparable to PECVD Si_3N_4.

Another problem in conventional poly-Si TFTs is the large off-state leakage of the transistors, due to field emission via grain boundary traps. By incorporating a lightly doped drain (LDD) region between the active channel and heavily doped source and drain regions, the electric field and thus the leakage current can be lowered. Fig. 3.5 depicts the process. In 3.5 a, the LDD doping level is set by a low-dose ion implantation while the polysilicon gate protects the underlying active channel region. Oxide spacers are then formed on both sides of the gate as described below. A high-dose ion implantation is then performed to form the highly doped source and drain regions, while the spacers protect the LDD (Fig. 3.5 c).

Conventional methods of forming the spacers include their definition by an extra lithographic step and etching, or the conformal deposition of a thick layer of oxide (Fig. 3.5 e) and anisotropic etch-back by reactive ion etching (RIE). During RIE the oxide is etched mostly in the vertical direction, and very little horizontally, so the spacers remain where the deposited oxide was thickest in the vertical direction (Fig. 3.5 f). Both methods have their problems—the lithographic method easily results in alignment errors, whereas the etchback method may cause plasma damage during RIE. A better alternative was proposed by Shih *et al.* [21, 25], who used LPD to grow an oxide sidewall spacer in a single step, requiring neither lithography nor etch-back (Fig. 3.5 b). The method relies on the selective nature of LPD, *i.e.* deposition occurs on the exposed side walls of the polysilicon gate, but not on the underlying Si_3N_4 film

or on the photoresist covering the gate.

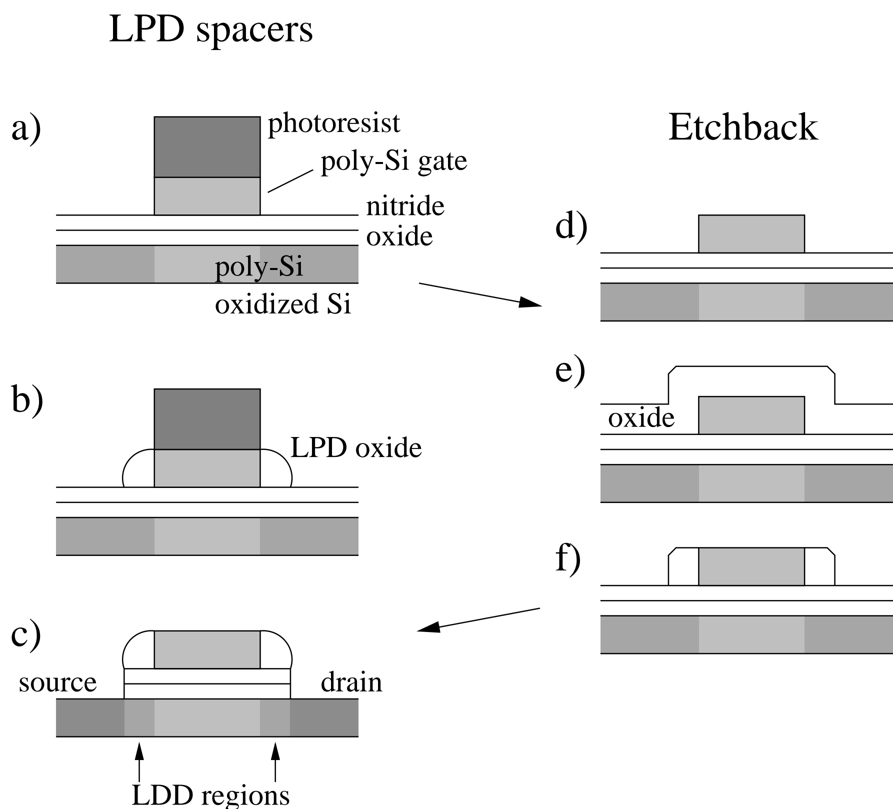

Figure 3.5: Formation of LDD spacers by LPD and deposition/etchback [21]. The shades of gray indicate the doping levels in the polysilicon layer.

3.5.2 Contact holes

The selectivity of LPD can be further utilized as an alternative method of patterning SiO_2 layers. Yeh *et al.* [24] demonstrate this with contact holes in n^+/p and Schottky diodes. Due to its anisotropic nature, RIE is usually used to open contact holes. RIE, however, causes surface damage and contamination of the underlying layers, and radiation damage resulting in fixed charge and SiO_2/Si interface traps. Also overetching can cause problems, particularly in ultra-shallow junction devices. Using LPD to form contact holes (Fig. 3.6) avoids all these problems. The diodes processed by Yeh *et al.* exhibited smaller reverse bias current and greater forward current density. In addition, the Schottky diodes formed by the LPD method performed reasonably well even before sintering, whereas the RIE samples required sintering to release residues and fix defects in order to work at all.

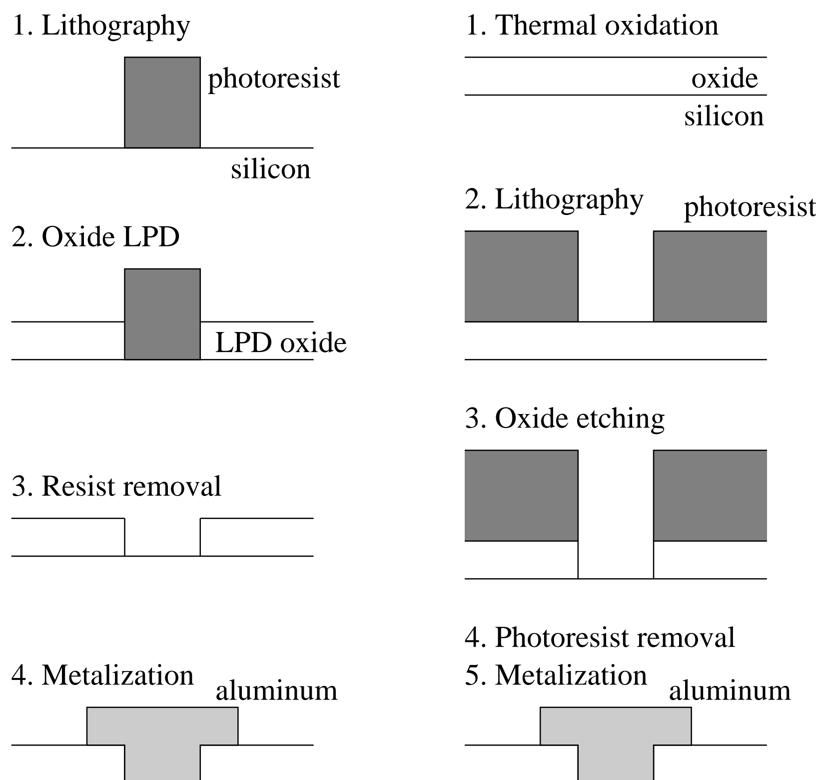

Figure 3.6: Two methods of contact hole formation [24]

3.5.3 CMOS

The low process temperature, selectivity and conformality of LPD can also be used to simplify CMOS processing. Kanba *et al.* [22, 23] report a simplified CMOS process using only 7 masks to first metalization (instead of a more typical 13 masks) utilizing LPD in photoresist mask reversal and in the formation of self-aligned sidewall spacers.

Fig. 3.7 shows the formation of adjacent n and p-type wells by ion implantation, using only a single mask. The n-well is implanted with phosphorous through a thin SiO_2 layer, while the p-region is shielded by the photoresist mask (3.7 a). A thick oxide layer is then deposited by LPD (3.7 b). Deposition occurs only on the unmasked areas, leaving a reverse polarity mask when the photoresist is removed (3.7 c). The p-wells are subsequently implanted with boron using the LPD oxide as a mask.

In the same CMOS process, the oxide spacers for LDD masking cannot be formed as in [21, 25] (Fig. 3.5 a–c) since the polysilicon gates are no longer covered with photoresist, and the underlying film is SiO_2 instead of Si_3N_4. Instead, the etch-back process (Fig. 3.5 d–f) is used, with the thick oxide being deposited by LPD.

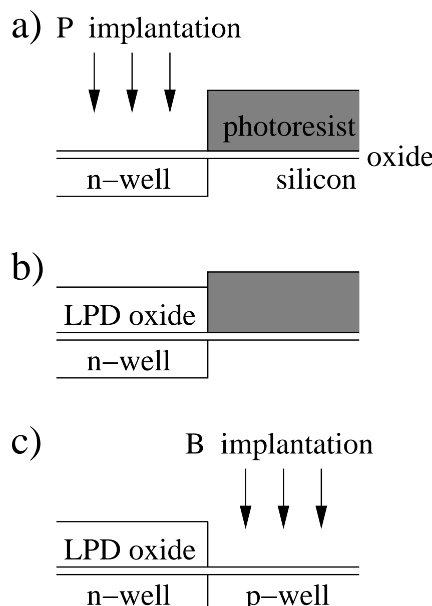

Figure 3.7: Formation of n- and p-wells for CMOS [23]

3.5.4 Planarization

Ultralarge-scale integrated devices often use multiple layers of metal wires to connect together different parts of the circuit. To maintain linewidth tolerances on the upper levels, a planar surface must be formed prior to metal deposition and patterning. Homma *et al.* [20] have developed a planarization method utilizing selective tungsten CVD and SiO_2 LPD. Fig. 3.8 outlines the process. The first metalization layer is deposited by sputtering and patterned by conventional RIE (3.8 a). SiO_2 is grown selectively by LPD over the underlying oxide, to the same height as the tungsten wiring, and the photoresist is removed (3.8 b). Next, a thin SiO_2 is deposited over the entire surface by PECVD, which acts as a seed layer for the deposition of a thick LPD oxide (3.8 c). LPD oxide is used because of its low dielectric constant and therefore smaller capacitance between metal layers. Via holes are etched by RIE and filled by selective CVD of tungsten (3.8 d), after which the second metal layer is sputtered and patterned as before (3.8 e).

Chen *et al.* [27] also propose a planarization technique based on SiO_2 LPD, suitable for planarizing inverted staggered TFTs to reduce their gate leakage current. When lower processing temperatures, thinner gate dielectrics and thicker gates are used, the leakage current increases at the corners of the gate where the insulator is thinnest as depicted in Fig. 3.9 e. This can be avoided by planarizing the structure prior to dielectric deposition, creating a uniform dielectric thickness, and therefore reduced gate leakage current. Fig. 3.9 depicts their process and the conventional inverted staggered TFT process. First the metal gate is greatly overetched (3.9 a) and SiO_2 is deposited by LPD. The thickness of the LPD SiO_2 film is greater than that of the gate, so the

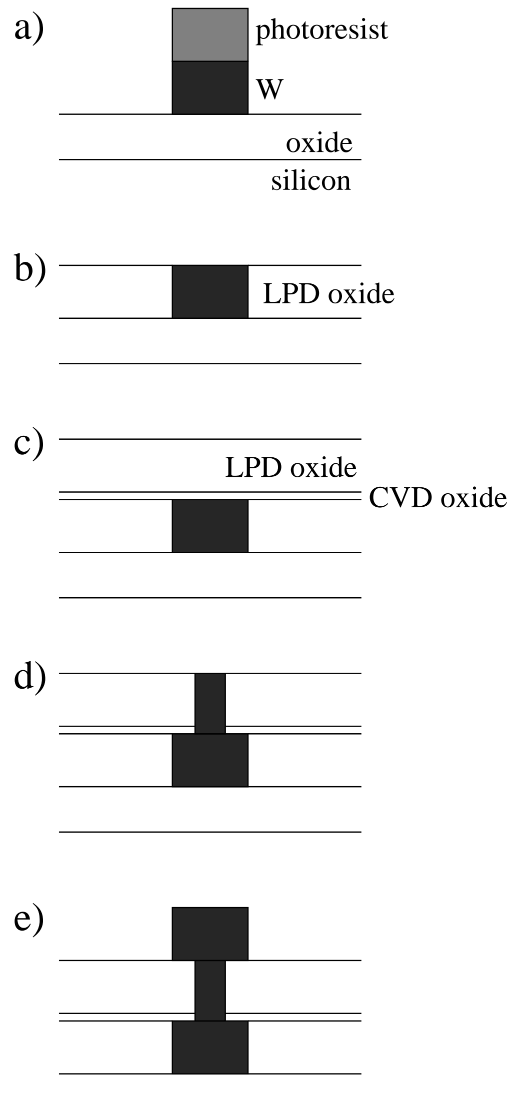

Figure 3.8: Multilevel planarization by LPD [20]

undercut beneath the photoresist is completely filled (3.9 b). After removing the photoresist, a planarized surface is exposed, over which the Si_3N_4 gate insulator, intrinsic a-Si:H and n-doped a-Si:H are grown by PECVD (3.9 c) and patterned into source and drain areas (3.9 d).

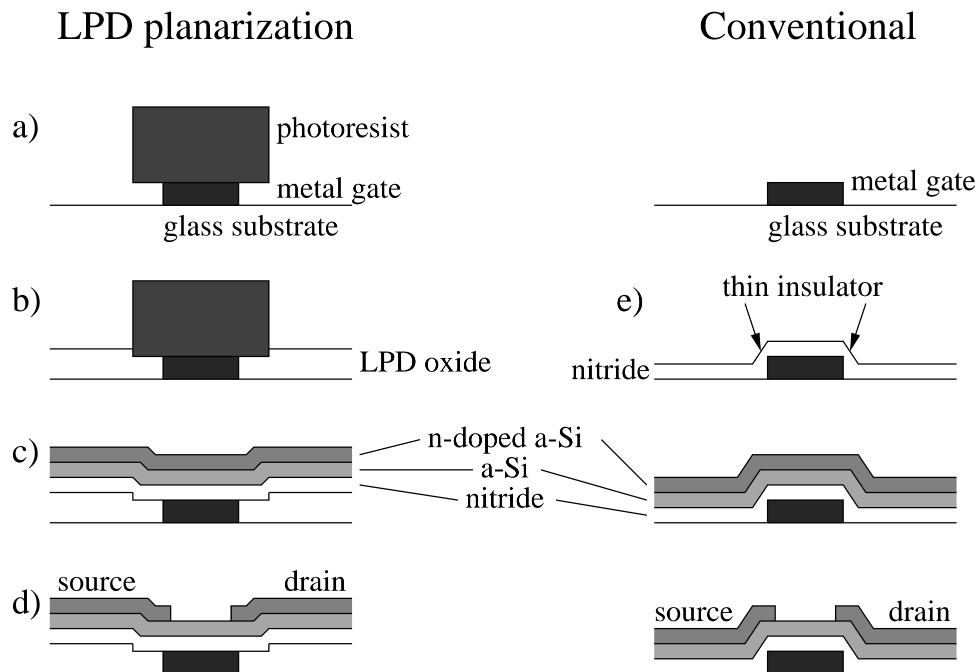

Figure 3.9: Inverted staggered TFT planarization by LPD [27]

Chapter 4

Experimental methods

4.1 Materials

100 mm single-side polished silicon wafers of (100) orientation were used as substrates for most depositions. In most cases the wafers were broken into pieces first.

Hexafluorosilicic acid (H_2SiF_6) was obtained as 25% (by weight) aqueous solution from Acros Organics, but later had to be changed to 35% solution from Lancaster Synthesis due to supply problems. 35% solution diluted with DI-water to 25% prior to saturation with SiO_2 was found to perform similarly to the original 25% solution. Hydrous SiO_2 (silicic acid, $SiO_2{\cdot}x\,H_2O$, Mallinckrodt Chemical) was used to saturate the H_2SiF_6 solutions. Boric acid ($>$99.5%, J. T. Baker) was dissolved in DI-water and diluted into stock solutions of 0.1 and 0.5 mol/dm^3 concentration.

AZ 5214E positive photoresist from Clariant was used for masking samples and lithographically patterning Si_3N_4-films. BHF, HF, other acids, acetone and isopropanol were all VLSI Selectipur grade chemicals from Merck. Evaporated metals were high purity, from various suppliers.

4.2 Equipment

The liquid phase depositions were carried out in a Teflon vessel on a standard magnetic stirrer-hotplate. For whole-wafer depositions, a 115 mm inner diameter × 190 mm high vessel was used, for smaller samples the respective dimensions were 75 mm × 110 mm. A Teflon-coated Pt-100 temperature probe was used to control the temperature with 1°C accuracy. The same magnetic stirrer was initially used for saturating the solutions with SiO_2, but an overhead stirrer was later substituted due to the rapid wear of the stirrer magnet's

Teflon coating. Polypropylene beakers were used in the saturation step and other steps where heating was not required. Glassware was avoided due to the corrosiveness of HF-based solutions, and to prevent unwanted deposition of SiO_2 from supersaturated solutions onto glass container walls.

Disposable 0.2 µm cellulose acetate filters from Schleicher & Schuell were used to filter SiO_2-containing H_2SiF_6 solutions. The solution was drawn into a 60 ml syringe, the filter was attached, and the solution was forced through the filter.

Photoresist masked samples were prepared by standard optical lithography using an Electronic Visions EV620 exposure tool with 1 µm minimum linewidth. Photoresist lines were thinned with oxygen plasma in an Oxford Plasma Technology reactor using 500 W power at 60 kHz and 86 sccm oxygen flow at 600 mTorr (80 Pa) pressure (see Appendix B). Thinning of photoresist was monitored with a Zeiss Axiospeed MCS 410 reflectometer at λ=380–760 nm. By repeatedly measuring a $\sim$1.4 µm thick photoresist sample at the same spot, the precision of the reflectometer was found to be on the order of 0.2%.

Silicon nitride samples were prepared by PECVD (Oxford Plasma Technology) using 100 W power at 1356 kHz and 600 mTorr (80 Pa) pressure. Two compositions of silicon nitride were prepared differing in stoichiometry (and therefore refractive index), with 150/2.5/350 sccm and 130/5/350 sccm $SiH_4/NH_3/N_2$ flow rates (SiH_4 was 1% in argon). Their refractive indices were 1.95 and 1.86, respectively. The Si_3N_4 samples were patterned by optical lithography and wet etching in BHF.

Copper, silver and gold patterns for testing the selectivity of SiO_2 LPD were prepared on silicon wafers by thermal evaporation with an Edwards E306A coating system. The sample was placed above a metal mesh acting as a shadow mask, so no lithography and etching was necessary for patterning. Chromium and tungsten were deposited by sputtering with an Oxford PlasmaLab System 400 sputter system. Chromium was patterned by optical lithography and wet etching with a solution of dilute perchloric acid and $Ce(NH_4)_2(NO_3)_6$, whereas tungsten could not be etched. The metal thicknesses, measured from patterned samples by profilometer, were on the order of 450 nm (silver), 250 nm (copper) and 100 nm (gold and chromium).

4.3 Deposition procedure

Hexafluorosilicic acid solution was saturated by adding SiO_2 and stirring for 24 hours or longer. When saturated solution was stored for later use, the SiO_2 powder was not removed, in order to ensure saturation even after extended storage. Prior to deposition, the growth vessel, stirrer magnet, temperature probe and sample holders were all soaked in BHF for several minutes and then rinsed with DI-water to ensure no SiO_2 particles were present.

The growth solution can be prepared in two ways (see Fig. 3.4 on page 13), denoted route I and route II. In route I, the H_2SiF_6 solution is first filtered, and then water and boric acid are added. In route II, water is added to the H_2SiF_6 solution already in the saturation stage, and no water is added to the solution after filtering. Both methods were tested, but route I was preferred since a smaller volume of liquid needs to be filtered.

The required amount of H_2SiF_6 solution was filtered directly into the growth vessel, and measured amounts of H_3BO_3 and water, mixed together, were added while stirring the solution. The solution was then heated to the desired temperature and samples were immersed for the desired time, while continuing to stir. After growth, the samples were rinsed in DI-water for five minutes and blown dry with nitrogen.

Where an oxide film of a given thickness was required, small reference samples were immersed in the growth solution together with the main sample. These were removed and their thickness measured before the expected growth time had expired. The total time required for the main sample was calculated from the reference samples' observed growth rates. Another possibility of monitoring film growth is to use a quartz crystal microbalance, as Deki *et al.* [46] reported for TiO_2 deposition. This approach was, however, not pursued here.

4.4 Characterization

Ellipsometry was the primary method for determining oxide film thickness and refractive index n. A Philips SD 2300 ellipsometer operating at λ=632.8 nm was used. The system offers two modes for measurement: floating n (where thickness and refractive index are calculated) and fixed n (where the refractive index is defined by the operator, and the thickness is calculated accordingly). The former was used for most measurements, while the latter was used for extremely thin films where the measured values of n may be unreliable. By repeatedly measuring a $\sim$35 nm LPD SiO_2 sample at the same spot, the precision of the ellipsometer was found to be on the order of 0.02% in both thickness refractive index.

A Dektak 3 profilometer was used to determine selectivity to silicon nitride by measuring the step height at the edge of the Si_3N_4 pattern before and after SiO_2 LPD. Selectivity to metals was determined by immersing the deposited sample in suitable acid solutions. Resistance to dissolution indicated overgrowth of SiO_2, whereas dissolution of the metal indicated selectivity to deposition. Since tungsten could not be etched, a photoresist pattern was formed on top, LPD was performed, followed by removal of the photoresist. The presence of a deposited film was tested by measuring for a step at the photoresist pattern edges with the profilometer.

A DSM-950 scanning electron microscope was used to examine photoresist-masked samples with thick layers of LPD-oxide. Widths of plasma-thinned photoresist lines were also determined by SEM. Most samples were sputter-coated with a few nanometers of gold prior to SEM-study.

The etch rate of the deposited oxide was measured in 1% (by weight) aqueous HF-solution and compared to the etch rate of thermal oxide in the same solution. Samples of oxide were etched for different lengths of time and their thicknesses before and after etching were measured by ellipsometer. Thicknesses were measured at several points and averaged. Since etching continues for a short time during rinsing of the sample, significant errors may result especially when very thin oxide films are being measured. These errors were avoided by plotting the etched thicknesses versus the etch time, and calculating the etch rate from the slope of this line.

To investigate the electrical properties of LPD SiO_2 films, MOS capacitor structures were fabricated (see Section 4.5). Their capacitances were measured with a Hewlett Packard 4192A LF impedance analyzer and their leakage currents and breakdown voltages with a Hewlett Packard 4155A semiconductor parameter analyzer.

4.5 MOS capacitor process

MOS capacitor structures with LPD SiO_2 dielectrics were fabricated on boron-doped silicon wafers of 0.02–0.03 Ω·cm resistivity. 72 nm of oxide was deposited from a solution of 150 ml 25% H_2SiF_6, 225 ml H_2O and 25 ml 0.1 mol/dm^3 H_3BO_3 at 35°C. The deposition time was 134 minutes. Photoresist was spun on the front side of the wafer, and the back side was etched free of oxide with BHF. The photoresist was removed first with acetone, then with isopropanol, in an ultrasonic bath.

200 nm of aluminum was sputtered on the front surface of the wafer. 500×500, 100×100 and 50×50 µm aluminum squares were patterned by optical lithography and etching with Merck PS 70-10 phosphoric acid etchant. Finally the photoresist was removed as before.

The substrate contact was made on the back side of the wafer by spreading a thin film of indium-gallium eutectic mixture, which is liquid at room temperature. The surface was then scratched thoroughly with a diamond scribe to break the native oxide layer. This way, a good electrical contact to the low-resistivity wafer was obtained.

Chapter 5

Experimental results

5.1 Growth rate

The average growth rates of LPD SiO_2 were determined under various growth conditions and with different growth solution compositions. Route I (see Section 3.3 or 4.3) was used to prepare the growth solutions. 25% H_2SiF_6 solution saturated with silicic acid was used in all experiments. The composition of the growth solution is given in terms of filtered H_2SiF_6 solution volume, volume of added 0.1 mol/dm^3 H_3BO_3 solution, and volume of added DI-water. The substrates were pieces of silicon wafer several cm in both dimensions. The thickness of the deposited SiO_2 was measured at several points on the substrate. This chapter presents only the general results obtained. The actual measurement data is included in Appendix A.

Significant variation was seen in deposition rates between experiments with identical growth solution compositions. Successive depositions from the same growth solution, however, showed good repeatability and very little decrease in deposition rate over time (indicating very little depletion of the growth solution due to deposition of SiO_2). Therefore to see the subtle effects of deposition temperature, water and H_3BO_3 additions, only a single growth solution was prepared for each experiment, and its composition or temperature was changed between depositions.

5.1.1 The effect of temperature

The effect of deposition temperature was investigated by performing 60-minute depositions at 25, 30, 35 and 40°C. The growth solution composition was 100 ml H_2SiF_6, 16 ml H_3BO_3 and 109 ml H_2O. Table 5.1 gives the results, which are presented graphically in Fig. 5.1.

Table 5.1: Effect of deposition temperature

Temp. (°C)	Rate (nm/h)	Refract. index
25	14.1	1.37
30	18.9	1.41
35	25.5	1.42
40	33.6	1.42

To obtain a rough estimate of the temperature sensitivity of the process, the above data is fitted to a linear regression model:

$$\frac{\text{Rate}}{\text{nm/h}} = \frac{\text{Temperature}}{^\circ\text{C}} \cdot 1.30 - 19.26$$

Variation in process temperature is under no circumstances expected to be worse than 1°C, so variation in the deposition rate due to temperature fluctuations is on the order of 1 nm/h. The sensitivity to temperature variation will increase with increasing process temperature, as the temperature dependence is not linear (see Fig. 5.1).

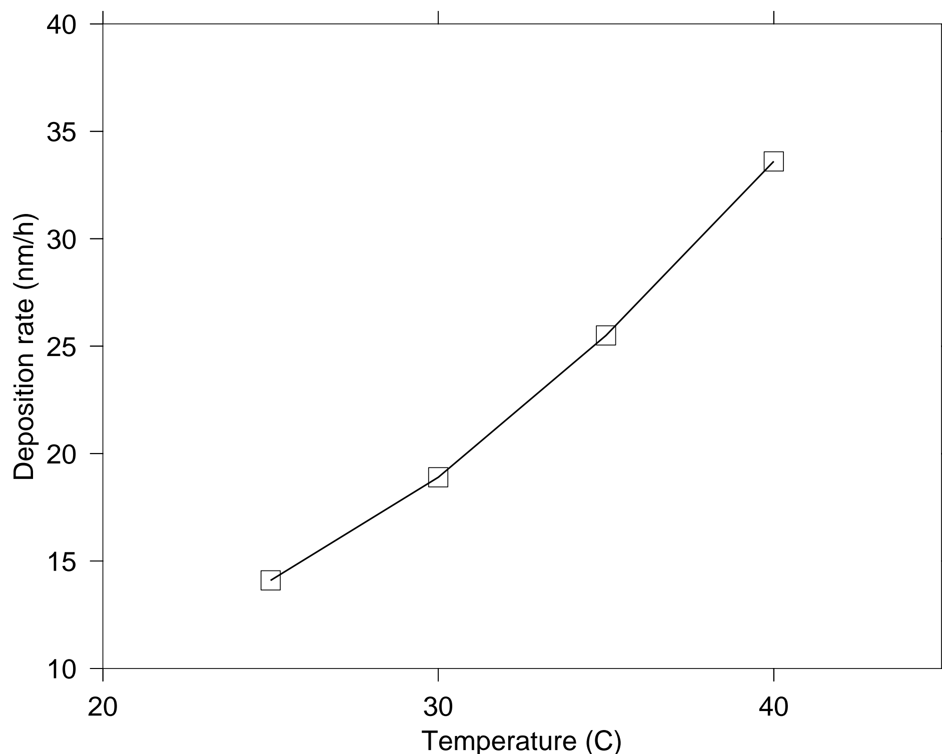

Figure 5.1: Effect of deposition temperature

The effect of deposition temperature may be due to two factors: shifting the equilibrium (reaction 3.1 on page 8) to the right according to Le Châtelier's principle, or increasing the reaction rate constant according to the Arrhenius equation:

$$k = Ae^{-E_a/RT} \tag{5.1}$$

To investigate the magnitude of these two factors, the following experiment was performed: First, 50 ml of saturated 25% H_2SiF_6 solution, 75 ml of H_2O and 8.3 ml 0.1 mol/dm^3 H_3BO_3 solution were used to perform a standard route I deposition at 35°C. Next, 25% H_2SiF_6 solution was saturated with SiO_2 by stirring >24 hours at the deposition temperature of 35°C. A growth solution of identical composition to the previous one was prepared, and deposition was carried out at the same 35°C. Finally, TD-LPD was attempted by simply saturating 25% and 35% H_2SiF_6 solutions with SiO_2 at room temperature and heating them to 35°C before deposition with no reagents added. Table 5.2 presents the results.

Table 5.2: Effect of temperature increase: oversaturation versus overall reaction rate

	Rate (nm/h)	Refract. index
Normal route I	18.83	1.46
Saturation at 35°C	17.72	1.47
TD-LPD, 35% H_2SiF_6	~3	—*)
TD-LPD, 25% H_2SiF_6	0**)	—*)

*) Measured using fixed $n = 1.465$

**) Native oxide is etched

Very little difference is observed in the growth rates with H_2SiF_6 solutions saturated at room temperature and at the final growth temperature. The deposition rate by only heating the solution was almost negligible for 35% H_2SiF_6, and 25% H_2SiF_6 actually etched the native oxide from the substrate. It can therefore be concluded that heating has very little effect on the equilibrium in the growth solution, but rather increases the overall rate of the reactions driven by the addition of water and/or H_3BO_3.

By writing the deposition rate as $r = kC$ where k is the reaction rate coefficient and C a factor incorporating the reagent concentrations in the solution, we can substitute k in equation 5.1 and rewrite it as:

$$\ln r = -\frac{E_a}{R} \cdot \frac{1}{T} + \ln A + \ln C \tag{5.2}$$

When the data in Table 5.1 is fitted to a linear model $\ln r = a \cdot \frac{1}{T} + b$, the activation energy $E_a = -a \cdot R = 45$ kJ/mol is obtained.

5.1.2 The effect of boric acid concentration

60-minute depositions were performed at 35°C to investigate the effect of boric acid addition. The solution composition was 100 ml H_2SiF_6 and 100 ml H_2O, with 0, 5, 10, 20 and 40 ml volumes of added H_3BO_3. Above this concentration, precipitation of SiO_2 was observed in the solution soon after H_3BO_3 addition. Table 5.3 shows the results which are presented graphically in Fig. 5.2.

Table 5.3: Effect of boric acid addition

H_3BO_3 addition		Deposition rate	Refract.
(ml added)	(mmol/dm^3)	(nm/h)	index
0	0	8.60	1.45
5	2.4	12.9	1.40
10	4.8	17.7	1.42
20	9.1	30.3	1.43
40	16.7	62.7	1.42

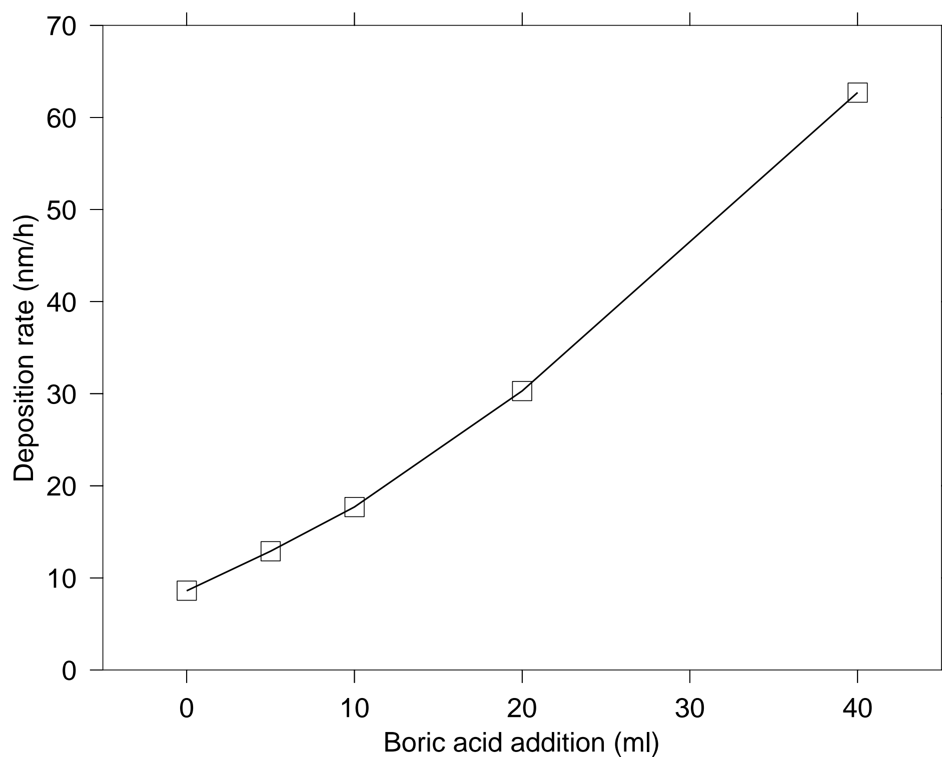

Figure 5.2: Effect of boric acid addition

Fitted to a linear regression model, the data yields:

$$\frac{\text{Rate}}{\text{nm/h}} = \frac{\text{H}_3\text{BO}_3\text{ volume}}{\text{ml}} \cdot 1.37 + 5.84$$

The volume of added boric acid can be controlled with better than 0.5 ml accuracy, so the variation in deposition rate should be less than 1 nm/h.

5.1.3 The effect of water addition

In a concentrated solution of H_2SiF_6, addition of a small amount of water can increase the water concentration of the solution without greatly reducing the H_2SiF_6 concentration. In a dilute H_2SiF_6 solution, on the other hand, addition of more water has little effect on the water concentration, but does further dilute the H_2SiF_6. Therefore, one would expect to find a certain optimum ratio of H_2SiF_6 to H_2O where the deposition rate is greatest.

To investigate the effect of the water concentration, depositions were performed by adding various amounts of water to 100 ml of saturated 25% H_2SiF_6 solution. H_3BO_3 was also added accordingly, to keep its concentration constant throughout the experiment. The same experiment was performed at several H_3BO_3 concentrations. The deposition temperature was 35°C throughout.

Table 5.4 summarizes the results. Results with an anomalously large deposition rate were always accompanied by a sharp decrease in refractive index, and have therefore been attributed to precipitation of oxide and have been removed from this table. The deposition rates are also plotted in Fig. 5.3.

Table 5.4: Effect of water addition

Deposition rate (nm/h)					
H_2O add. (ml)	Total H_3BO_3 concentration ($mmol/dm^3$) 3.2	6.3	9.1	12.0	
50	9.26	15.5	18.2	30.7	
100	15.3	22.1	26.8	40.8	
150	17.0	23.1	29.3	41.1	37.8
200	16.3	21.5	27.9		38.4
250	15.0	19.8	26.1		
300	13.6				

Except for the results using the highest concentration of H_3BO_3, where precipitation caused problems already in the early stages of deposition, there is a clear maximum in deposition rate around the 150 ml H_2O:100 ml H_2SiF_6 ratio (corresponding to 0.88 mol/dm^3 H_2SiF_6 concentration). This ratio appears independent of the H_3BO_3 concentration.

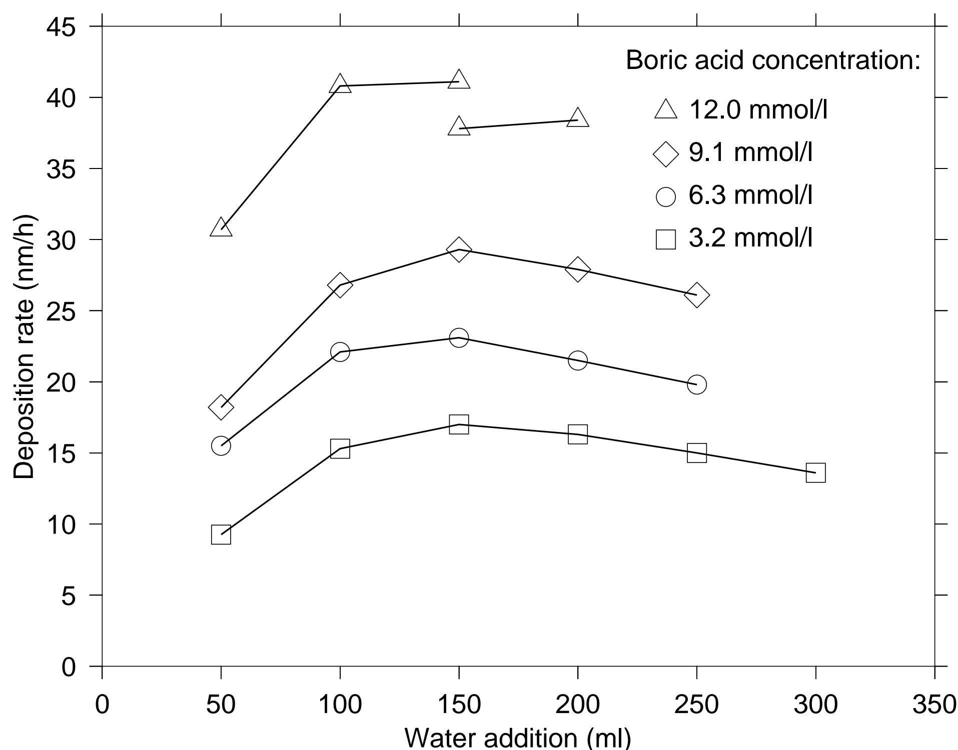

Figure 5.3: Effect of water addition

5.1.4 The effect of the initial H_2SiF_6 concentration

The deposition rate using 35% H_2SiF_6 solution is vastly greater than with 25% solution under the same conditions, and SiO_2 also begins to precipitate more easily. A growth solution with 50 ml 35% H_2SiF_6, 50 ml H_2O and 5 ml H_3BO_3 at 35°C begins to precipitate in less than 60 minutes and produces visibly cloudy films. However, if no H_3BO_3 is added, or if the deposition is performed at room temperature (about 20°C), better films are obtained. Some results are presented in Table 5.5.

Table 5.5: Growth rate from 35% H_2SiF_6 solution

Temp. (°C)	35% H_2SiF_6 (ml)	H_2O (ml)	H_3BO_3 (ml)	Rate (nm/h)	Refract. index
35	50	27	0	37.0	1.43
RT*)	25	13.5	0	5.1	—**)
RT	25	13.5	2	57.8	1.43
RT	25	9	4.5	19.2	1.43
RT	25	45	2.5	25.8	1.44

*) Room temperature, ≈20°C

**) Measured using fixed $n = 1.465$

If 35% H_2SiF_6 is diluted to 25% before saturating it with SiO_2, similar results are obtained as with the original 25% H_2SiF_6 solution—the observed difference in deposition rate is within the variation range typically seen with 25% solutions.

5.2 Film characteristics

5.2.1 Refractive index and thickness uniformity

The first indicator of film quality is its refractive index. The refractive index of thermal SiO_2 is 1.465 [37]. For LPD SiO_2 the refractive index is typically slightly less, around 1.42–1.43. A sharp decrease in refractive index is observed immediately before SiO_2 begins to precipitate in the growth solution and deposited films become cloudy. Thus a refractive index of less than 1.4 serves as an effective warning that the deposition was not necessarily successful, even if the film is visually clear.

The uniformity of the deposited film is excellent. To gain some idea of the feasibility of batch-processing by LPD, two whole wafers were attached to a sample holder with about 5 mm distance between the wafers. They were then immersed face down in LPD growth solution in a 115 mm inner diameter beaker with a magnetic stirrer on the bottom. Using 150 ml H_2SiF_6, 225 ml H_2O and 25 ml H_3BO_3 at 35°C, a 63 minute deposition was performed, yielding about 35 nm of oxide (see Table 5.6). The standard deviation of the oxide thickness (measured at 37 points on the wafer) was only 0.3% for the bottom wafer (closer to the magnetic stirrer), and 0.5% for the top wafer (receiving considerably less circulation of the growth solution). Also the difference in deposited oxide thickness between the two wafers was only 1%. All these numbers compare very well even to thermal oxidation, and indicate the excellent suitability of LPD for batch processing.

Table 5.6: Uniformity of the deposited oxide on a whole 100 mm wafer

	Thickness			Refractive index		
	AVG	STDEV		AVG	STDEV	
	(nm)	(nm)	(%)			(%)
Bottom wafer	35.27	0.11	0.3	1.4302	0.0028	0.2
Top wafer	34.89	0.18	0.5	1.4287	0.0031	0.2

It is important to note that all depositions have been carried out on substrates with a native oxide on the silicon surface. If this oxide is removed by dipping in dilute HF immediately before deposition, very poor thickness uniformity is obtained. Under the same conditions (100 ml H_2SiF_6, 16 ml H_3BO_3, 134 ml H_2O, 35°C, 90 minutes) the SiO_2 film deposited on a HF-dipped sample

is significantly thinner than on a sample with the native oxide present, and exhibits 10 times greater standard deviation in thickness (Table 5.7). This indicates delayed onset of deposition on a bare silicon surface. Once deposition does begin, however, the quality of the deposited oxide is good, as can be seen from its refractive index.

Table 5.7: Uniformity of the deposited oxide on native oxide and bare silicon

	Thickness			Refractive index		
	AVG	STDEV		AVG	STDEV	
	(nm)	(nm)	(%)			(%)
Native oxide	40.5	0.1	0.3	1.4390	0.0021	0.1
HF-dipped	32.3	1.4	4.2	1.4335	0.0083	0.6

5.2.2 Etch rate in HF

Table 5.8 presents the results of etching thermal and LPD oxide in 1% HF. The LPD oxide results are also shown in Fig. 5.4, and exhibit good linearity with a slope (*i.e.* etch rate) of 0.48 nm/sec or 29 nm/min. The measured etch rate of thermal oxide is considerably less, *viz.* 4.8 nm/min.

Table 5.8: Thicknesses of thermal and LPD oxide samples before and after etching in 1% HF.

		Thickness (nm)		Etched
	Etch time	before	after	thickness (nm)
Thermal oxide:	5 min	185	159	26
	10 min	183	127	56
	15 min	180	104	76
	20 min	183	84	99
LPD oxide:	10 sec	34.9	30.1	4.8
	20 sec	34.6	24.9	9.7
	40 sec	34.8	15.5	19.3

5.2.3 Electrical characteristics

MOS-capacitors of three different sizes were measured at 100 kHz frequency, 0.1 V amplitude and zero bias voltage. The capacitances of several capacitors were averaged, and from these values the dielectric constant ϵ of the oxide layer was calculated according to the equation:

$$C = \frac{\epsilon \epsilon_0 A}{d} \tag{5.3}$$

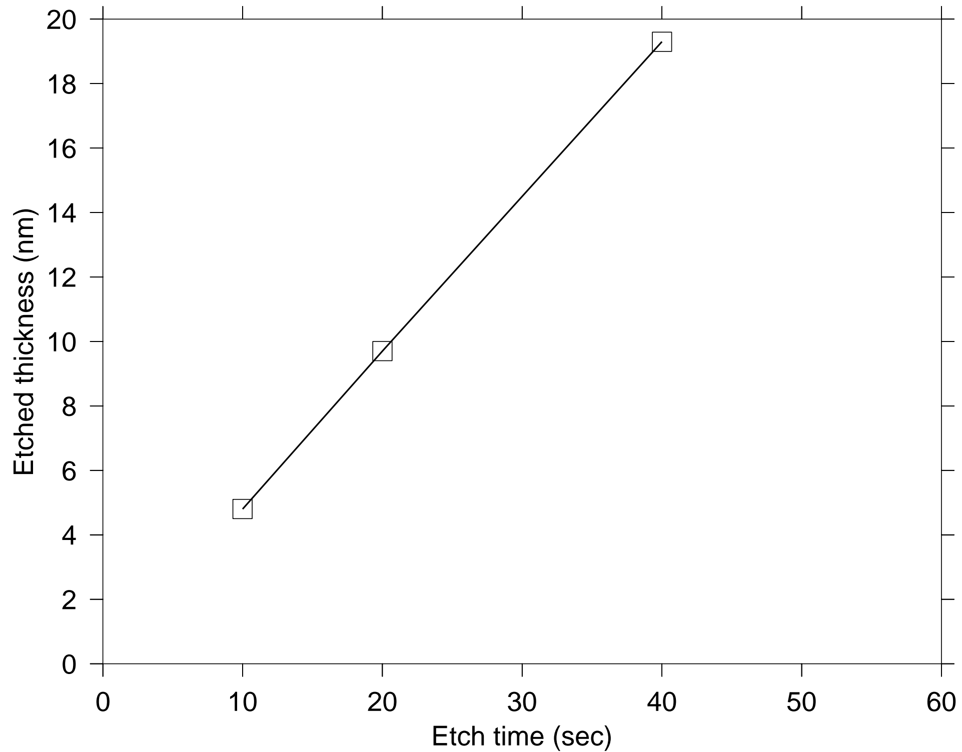

Figure 5.4: Etched thickness of LPD oxide versus time in dilute HF

where C is the capacitance, $\epsilon_0 = 8.854 \cdot 10^{-12}$ F/m is the permittivity of space, A the area of the capacitor, and $d = 72 \cdot 10^{-9}$ m the thickness of the dielectric. The results are tabulated in Table 5.9.

Table 5.9: Capacitances of MOS capacitors and the calculated dielectric constants of LPD SiO_2

Capacitor			
dimensions	area	Capacitance	ϵ
500×500 µm	$250{\cdot}10^{-9}$ m^2	165 pF	5.4
100×100 µm	$10{\cdot}10^{-9}$ m^2	6.53 pF	5.3
50×50 µm	$2.5{\cdot}10^{-9}$ m^2	1.62 pF	5.3

To determine the breakdown voltage of a capacitor's dielectric, the voltage across the capacitor was ramped up from zero at 0.77 V/sec until a sharp, sudden increase in leakage current indicated dielectric breakdown, as in Fig. 5.5. The measurement was performed on the largest two sizes of capacitors, on a sampling of 30 each. The cumulative failure percentages are plotted against the electric field in Figs 5.6 and 5.7 (the actual breakdown voltages are listed in Tables A.9 and A.10 in Appendix A).

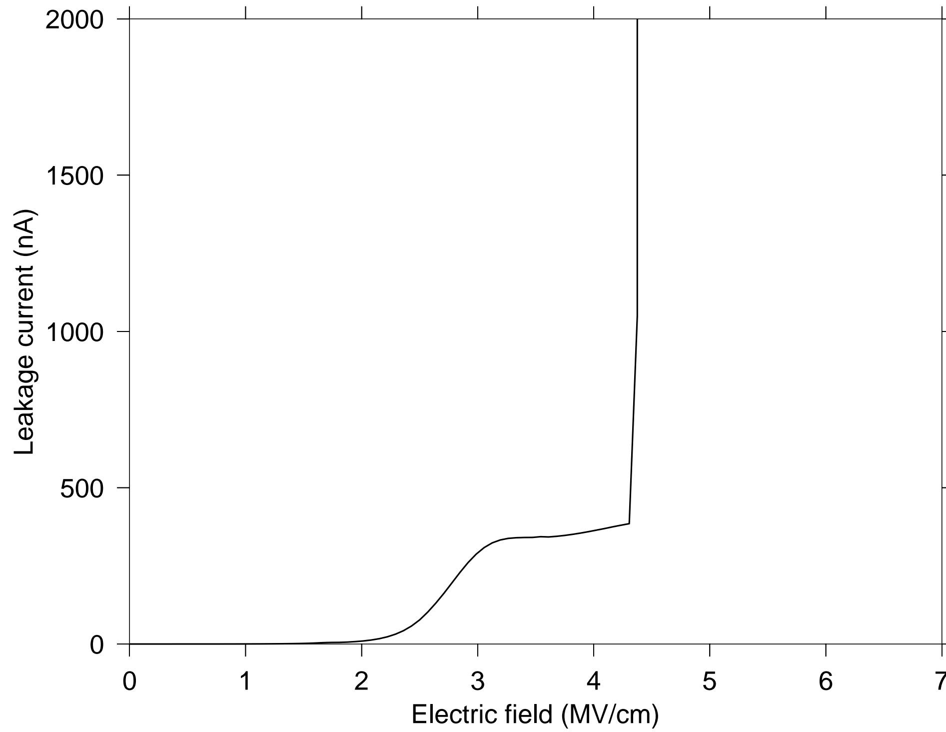

Figure 5.5: Dielectric breakdown of a MOS capacitor

For the larger capacitors (Fig. 5.6), some failures are observed already around 1 MV/cm. These may be due to individual defects in the oxide film, whereas the intrinsic breakdown electric field of the oxide is on the order of 4 MV/cm, where a notable rise in the number of failures is seen. This interpretation is supported by the fact that a smaller number of defect-induced failures is seen for the smaller capacitors (Fig. 5.7), since they have a smaller surface area and are therefore less likely to contain a major defect.

The leakage current density of the oxide was measured at 2 MV/cm (14.3 V for the 72 nm dielectric). All three sizes of capacitors were measured, however the validity of the results obtained with the smallest capacitors is questionable. The smaller average leakage current of the 100×100 µm capacitors may be explained by individual defects as above. The measurement setup exhibited a parasitic leakage current of 17.5 pA which has been corrected for in the results presented in Table 5.10.

Table 5.10: Leakage current densities in LPD SiO_2 at 2 MV/cm

Capacitor		Leakage	Leakage
dimensions	area	current	current density
500×500 µm	$250 \cdot 10^{-9}$ m^2	1810 pA	724 nA/cm^2
100×100 µm	$10 \cdot 10^{-9}$ m^2	50.4 pA	504 nA/cm^2
50×50 µm	$2.5 \cdot 10^{-9}$ m^2	27.9 pA	1110 nA/cm^2

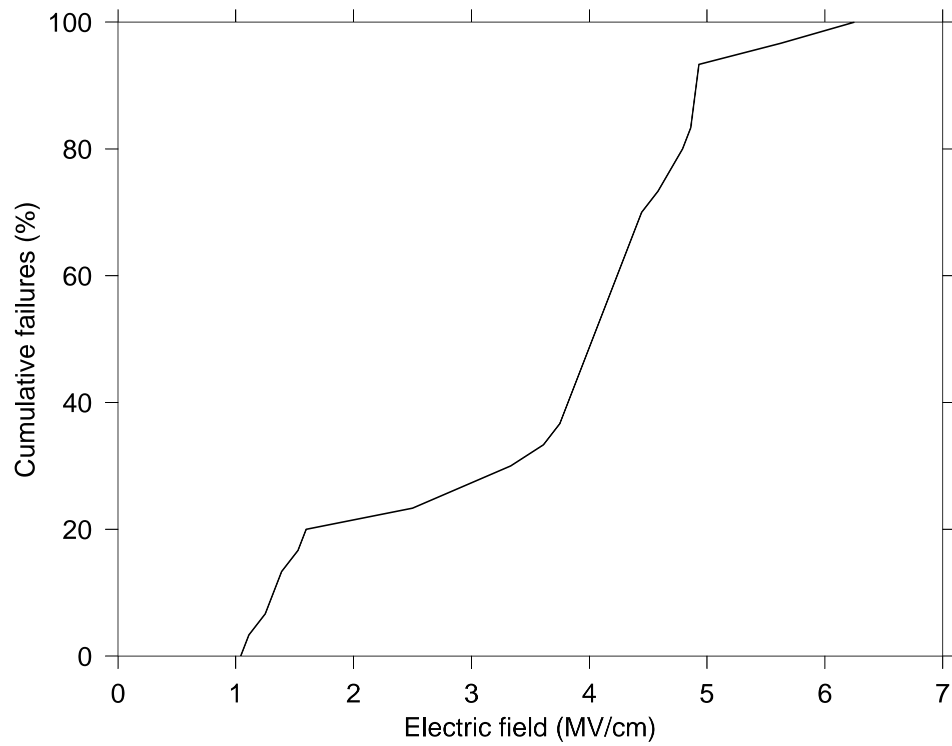

Figure 5.6: Cumulative failure percentage as a function of applied electric field: 500×500 µm capacitors

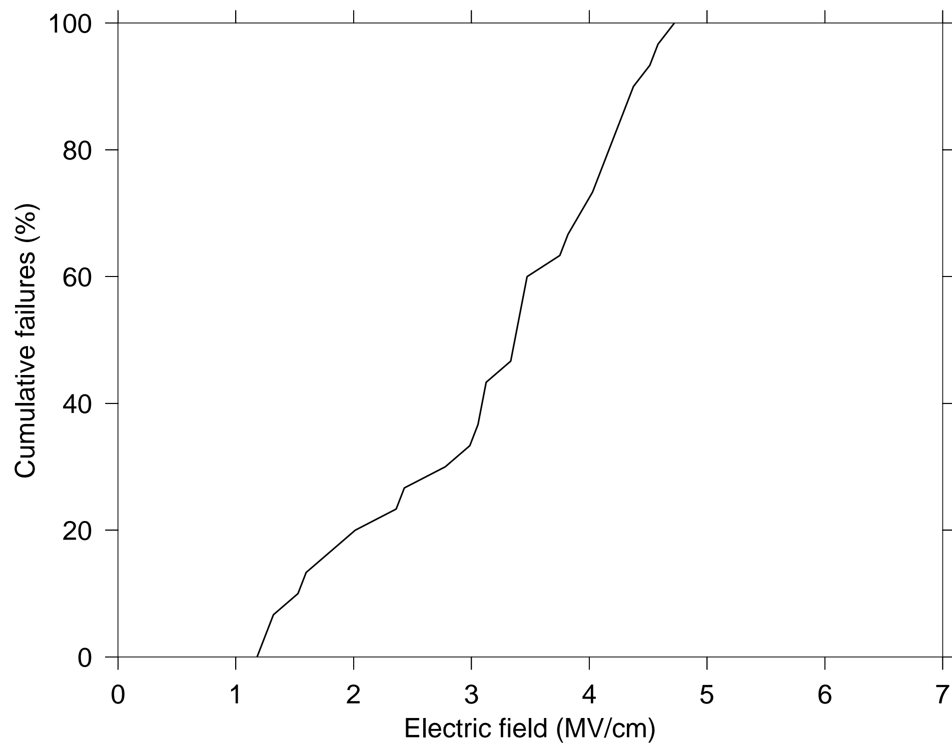

Figure 5.7: Cumulative failure percentage as a function of applied electric field: 100×100 µm capacitors

5.3 Selectivity of deposition

Observed selectivity of SiO_2 LPD on various materials is presented in Table 5.11. Bare silicon with its native oxide removed by HF treatment exhibits delayed growth, as noted previously (Section 5.2.1). Both nitride compositions (see Section 4.2) were tested for selectivity, but no difference between the two was seen, and oxide was deposited on both. Aluminum dissolves in the growth solution, since it reacts with HF (Section 3.1).

Table 5.11: SiO_2 deposition on various materials

Material	Deposition?
Silicon (native oxide)	Yes
Silicon (HF-dipped)	Delayed
Silicon dioxide	Yes
Silicon nitride	Yes
Photoresist	No
Photoresist (plasma thinned)	No
PMMA	No
Aluminum	Dissolves
Chromium	No
Copper	No
Silver	No
Tungsten	Yes
Gold	Yes

5.4 Maximum thickness of LPD SiO_2

A major problem found to occur in LPD is liquid phase nucleation and subsequent precipitation of SiO_2 in the growth solution. Contrary to the claim of Chang *et al.* [31] that the solution stays clear indefinitely below a certain boric acid concentration, precipitation does eventually occur even at a low H_3BO_3 concentration. Particles are typically observed at the surface of the solution already after $<$4 hours. At this point, a clear laser spot is visible on the surface of the substrate during ellipsometer measurement, indicating some surface roughness. Continued deposition results in precipitation within the solution and visibly clouded films. 100 nm has been found to be the practical upper limit obtainable in a single deposition, about 60 nm if no surface roughness is tolerated.

As precipitation in the solution begins, particles are deposited on the substrate and included in the growing SiO_2 film, causing cloudiness and a decrease in refractive index. Particles may also be deposited on photoresist films or other

mask materials on the substrate, causing LPD SiO_2 overgrowth. The SEM image in Fig. 5.8 shows a hollow structure formed by overgrowth on photoresist, followed by photoresist removal in acetone. Since oxide deposition continues between and around the precipitated SiO_2 particles, such composite films may be structurally sound and quite dense and conformal. In fact, standing wave patterns on the sidewalls of photoresist lines have been seen faithfully reproduced in particle-filled LPD SiO_2 deposits.

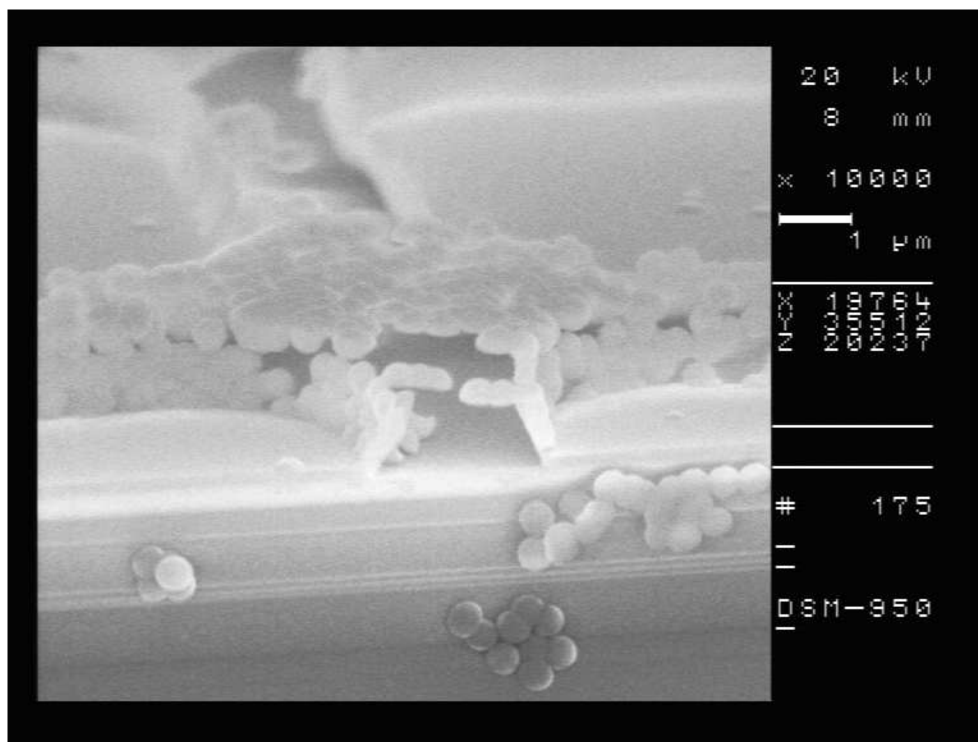

Figure 5.8: Precipitation of oxide in the growth solution has caused SiO_2 overgrowth on photoresist lines. The photoresist has subsequently been removed.

The addition of water without boric acid was found not to cause significant oxide deposition. However, the addition of a large amount of water into a saturated H_2SiF_6 solution could cause a momentary, but substantial supersaturated state. This supersaturated state would not last long, but might trigger the formation of nano-crystals of silicon dioxide in the solution. These crystals would later act as centers for precipitation.

LPD by route II (Section 3.3) was therefore investigated as a possible solution to the precipitation problem. However, signs of beginning precipitation were evident in the growth solution already after 4 hours (80 nm) deposition, with the ellipsometer's laser spot clearly visible on the sample during measurement. As the choice of solution preparation route does not appear to affect the onset of precipitation, route I may be preferred since a smaller amount of liquid needs to be filtered.

Chapter 6

Image reversal

As mentioned in Section 2.3, ECR plasma oxidation has been used by Kurihara *et al.* [7] to reverse the polarity of a photoresist image. The image is formed by EBL over an amorphous silicon layer, which is selectively oxidized in the plasma where not protected by the resist pattern. The 2–3 nm thick oxide pattern formed in the surface of the *a*-Si is the reverse image of the photoresist mask, and can be transferred into the *a*-Si by etching. The *a*-Si pattern in turn is transferred into an underlying thicker oxide layer, which is the final reversed oxide mask.

LPD can also be used to reverse the polarity of a photoresist mask, due to the selectivity of deposition. The advantage of LPD, compared to the plasma oxidation process, is not requiring the deposition and etching of multiple layers of *a*-Si and oxide. Instead, the reversed oxide mask is formed in a single deposition step, followed by removal of the photoresist.

The possibility of image reversal becomes more interesting when combined with other post-lithography processing of the photoresist image. An example of such processing is thinning of photoresist lines by oxygen plasma ashing. Normally, the line width in optical lithography is limited by the wave length of the exposing radiation. However, thinner lines can be made by isotropically etching the organic photoresist in an oxygen plasma (plasma ashing). This method was developed by Chung *et al.* [47] to produce 0.2 µm MOS-devices using *g*-line (λ=436 nm) optical lithography. Sub-30-nm devices have been demonstrated by Asano *et al.* [48] in conjunction with *i*-line (λ=365 nm) and e-beam lithography.

The plasma ashing process is restricted to light-field structures (lines and dots) only. Dark-field structures (trenches and holes) are widened (see Fig. 6.1). However, image reversal can extend the process to dark-field structures [49]. To demonstrate this, 2 µm wide photoresist lines were thinned to 200 nm in an isotropic oxygen plasma. Fig. 6.2 shows such a line. Residues from the plasma ashing process are visible surrounding the line, but they were not found to present a problem during SiO_2 deposition.

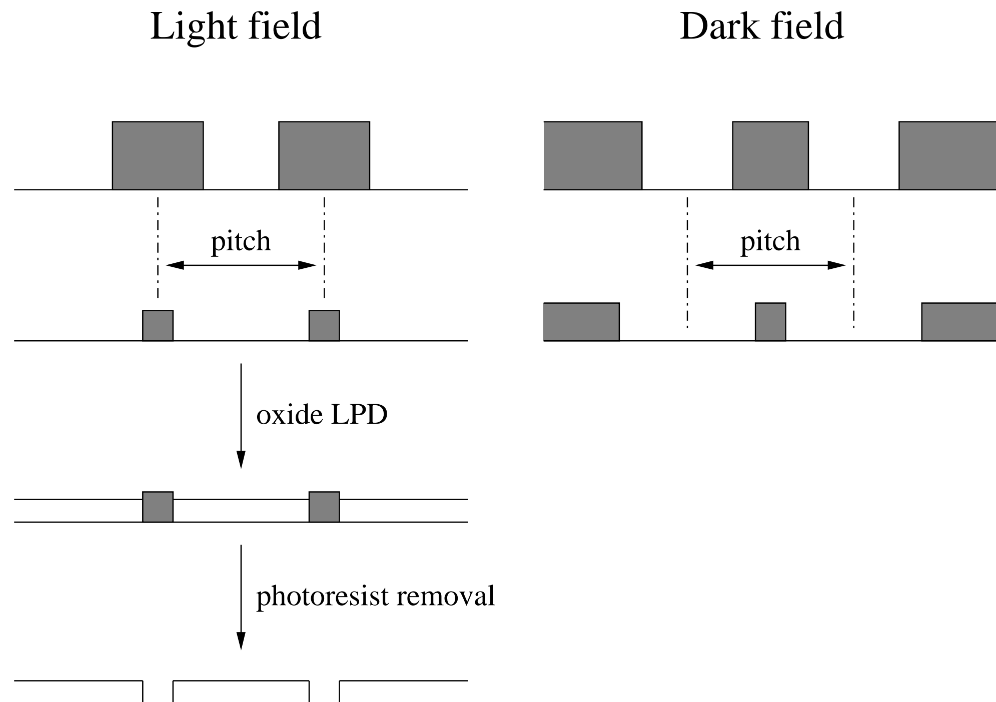

Figure 6.1: Photoresist thinning by oxygen plasma ashing

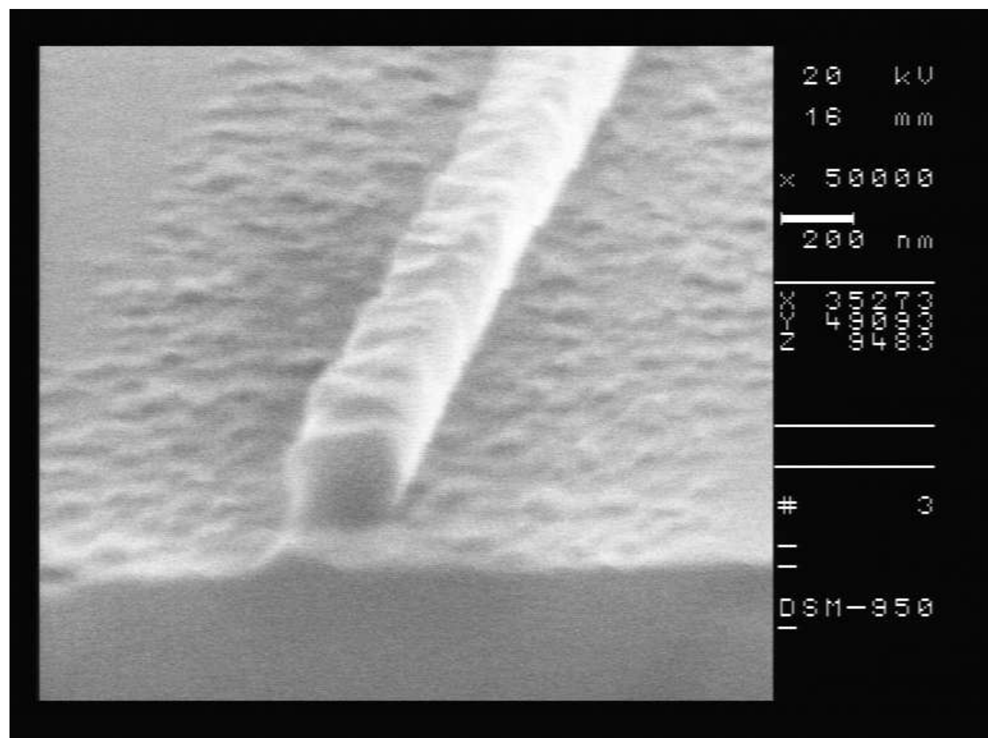

Figure 6.2: 200 nm wide photoresist line prepared by plasma ashing

Details of the plasma ashing process are presented in Appendix B. It must be noted that thinning photoresist lines from 2 µm to 200 nm constitutes a 90% reduction in line width and cannot be expected to be a repeatable process. In practice, a 50% reduction may be more realistic. In this work, ultimately thin lines were fabricated only to demonstrate the feasibility of image reversal by LPD on a deep sub-micron scale. It should also be pointed out that plasma ashing affects only line width, not line pitch, as is seen from Fig. 6.1. Thus dense arrays of thin lines cannot be fabricated by this process.

Next, a ~60 nm thick LPD oxide was deposited using the thinned photoresist pattern as a mask. The photoresist was finally removed with acetone and isopropanol in an ultrasonic bath, leaving 200 nm wide trenches in the oxide (Fig. 6.3). The particles seen on the sample surface are probably deposited during photoresist removal, which was done outside the clean room. Similar particles are seen in Fig. 6.4 in areas that were masked during SiO_2 deposition, so they are not believed to be precipitated oxide.

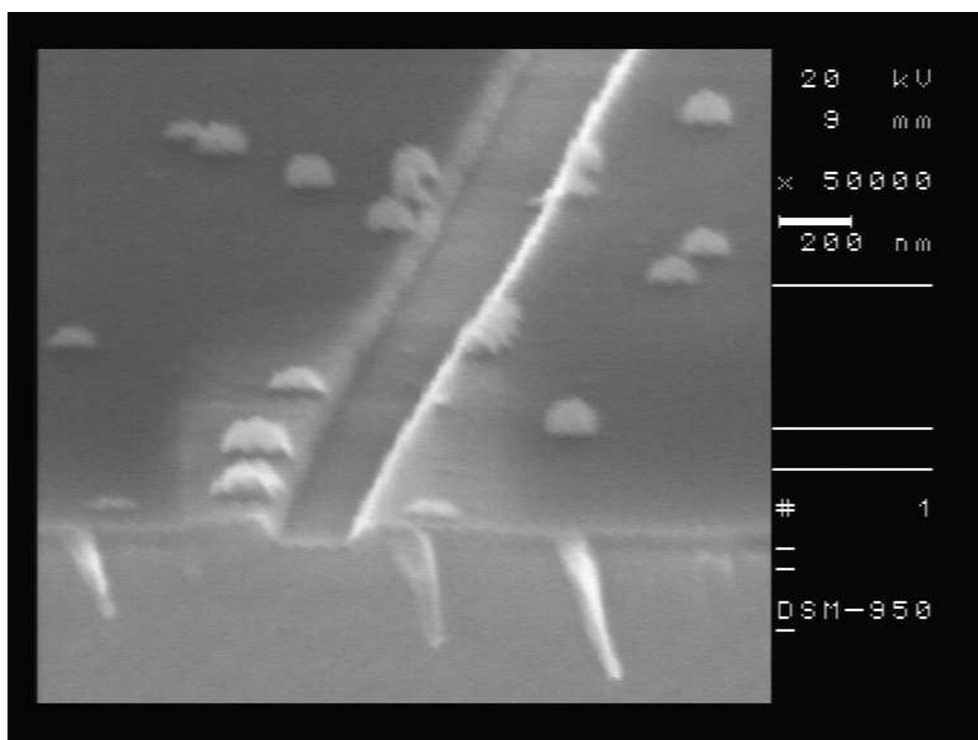

Figure 6.3: 200 nm wide trenches in LPD oxide

Image reversal by LPD was also attempted using a PMMA mask patterned by electron-beam lithography. 200 nm wide openings were made in the dark-field mask. The sample was then directly immersed in LPD growth solution, and after deposition the PMMA mask was removed as before. Fig. 6.4 shows 200 nm wide oxide lines which accurately reproduce the original pattern.

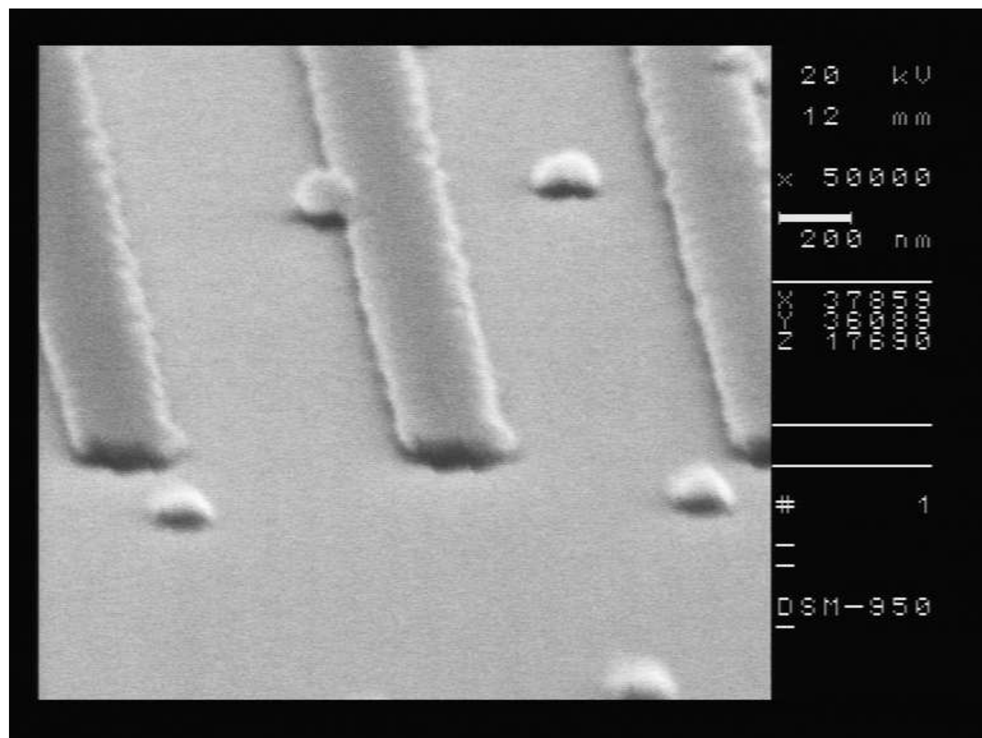

Figure 6.4: SiO_2 lines formed by reversal of EBL-defined dark-field structures

Chapter 7

Conclusions

Liquid phase deposition of silicon dioxide from an aqueous solution of hexafluorosilicic acid H_2SiF_6 by the addition of boric acid H_3BO_3 was studied. A suggested recipe for SiO_2 LPD is presented and the main results are summarized in this chapter.

7.1 Recommended recipe for SiO_2 LPD

A method for depositing good quality SiO_2 films by LPD is presented in the following.

1. Saturate a sufficient volume, over 150 ml, of 25 weight-% aqueous H_2SiF_6 solution by adding ample silicic acid ($SiO_2 \cdot xH_2O$) powder and stirring overnight at room temperature (~20°C) with an overhead stirrer, using only polypropylene or Teflon materials wherever in contact with the solution. The saturated solution may be stored for later use if the undissolved SiO_2 powder is not removed.
2. Soak the Teflon vessel, magnetic stirrer bead, Teflon-coated temperature probe and sample holder in BHF for several minutes to remove any SiO_2 deposits from previous depositions. Rinse thoroughly with DI-water.
3. Filter 150 ml of saturated H_2SiF_6 solution through a 0.2 µm membrane filter into the reaction vessel.
4. Mix together 25 ml of 0.1 mol/dm^3 boric acid solution and 225 ml water, and add them to the H_2SiF_6 solution while stirring.
5. Heat the solution to 35°C with constant stirring and immerse the substrate for deposition. After deposition rinse with DI-water.

Thus the recommended composition for a growth solution is:

- 150 ml saturated and filtered 25% H_2SiF_6 solution
- 225 ml DI-water
- 25 ml 0.1 mol/dm^3 H_3BO_3 solution

This growth solution volume is sufficient for deposition on two 100 mm wafers simultaneously, when the wafers are placed horizontally in a 115 mm inner diameter vessel. The reagent volumes can be scaled as required to cover the substrates completely in different deposition geometries. At 35°C deposition temperature the deposition rate is on the order of 30 nm/h. To obtain a specified oxide thickness, reference samples should be used to determine the exact deposition rate during LPD.

If room-temperature processing is preferred, or addition of H_3BO_3 should be avoided, 35% H_2SiF_6 solution is more suitable than 25% solution to maintain good film quality (see Table 5.5 in Section 5.1.4). Temperature-dependent LPD (TD-LPD) was not attempted with saturation below room temperature. Saturation at room temperature and deposition at 35°C does not result in enough supersaturation to make TD-LPD possible (see Section 7.5).

7.2 Film properties

Silicon dioxide thin films up to 100 nm in thickness can be grown in a single deposition step by liquid phase deposition. The growth rate depends on the composition of the solution, especially the concentration of boric acid. Using 25% H_2SiF_6, the greatest growth rate is achieved at 150 ml H_2O:100 ml H_2SiF_6 (0.88 mol/dm^3 overall H_2SiF_6 concentration), whereas increased H_3BO_3 concentration always increases the deposition rate. The refractive index of the deposited oxide is typically around 1.43, slightly lower than that of thermally grown oxide. Thickness uniformity on a 100 mm wafer is excellent, exhibiting typically less than 0.5% standard deviation.

The etch rate in 1% hydrofluoric acid was found to be about six times greater than that of thermal oxide. This is a significant difference, and indicates either a porous structure or a high concentration of dangling or terminating bonds. Densification of the film by thermal annealing might improve its properties and should be investigated if LPD oxide is to be used as any kind of etch mask.

Working MOS capacitors were fabricated and used to investigate the electrical properties of LPD SiO_2 deposited using the recipe mentioned earlier. The measured dielectric constant ϵ=5.3 is notably higher than any published previously, and should be regarded with suspicion as it may be affected by factors

such as film roughness. The intrinsic dielectric breakdown electric field of 4 MV/cm is lower than published elsewhere. Better dielectric strength may be obtained by optimizing specifically for that purpose, though film roughness may also have an effect here. The leakage current density of the film is comparable to that reported by Yeh *et al.* [18].

7.3 Selectivity of deposition

Deposition occurs readily over existing silicon dioxide. A native oxide layer is sufficient for the onset of deposition. On bare silicon, stripped of its native oxide, uneven films are deposited, presumably due to delayed growth.

Contrary to reports found in literature, LPD SiO_2 was found to grow over silicon nitride. The nitride films used in this study were deposited by PECVD, whereas other investigators have used LPCVD-deposited films. This may well be an important factor, since the two are notably different *e.g.* in their etching properties—PECVD nitride dissolves readily in BHF (which was used for patterning here), whereas LPCVD nitride is almost insoluble in HF and BHF.

No deposition occurs on photoresist, either immediately after lithography or after extensive oxygen plasma ashing. PMMA was also found to resist deposition. This selectivity makes possible the use of LPD for reversal of photoresist masks.

Also, deposition does not occur on some metals, *i.e.* chromium, copper or silver. SiO_2 is, however, deposited on gold and—contrary to several published reports—tungsten.

7.4 Image reversal

The selective nature of LPD was utilized for image reversal of photoresist masks. Since deposition occurs on silicon but not on photoresist, a reverse image remains when photoresist is removed. When combined with photoresist line-width thinning by oxygen plasma ashing, sub-lithographic dark-field patterns (trenches and holes) can be produced in the oxide film. This novel mask-formation method was demonstrated on a deep sub-micron scale and was presented by the present author at the Micro and Nano-Engineering 2000 International Conference [49]. The same method can be used to reverse images defined in PMMA resist by electron beam lithography.

7.5 Temperature effects

The TD-LPD method demonstrates that significant supersaturation of the growth solution can result from heating the solution—enough, in fact, for deposition without addition of any water or boric acid. This, however, requires saturation at a very low temperature (around 0°C), which was not attempted here. TD-LPD with saturation at room temperature and subsequent heating to 35°C resulted in little or no deposition, or even etching of existing native oxide. Conversely, conventional LPD was very little affected by changing the saturation temperature from room temperature to 35°C (same as the deposition temperature). It can therefore be concluded that in this temperature range, little or no supersaturation results from the temperature change. Rather, the observed increase in deposition rate with increasing temperature is attributed to a greater reaction rate coefficient, in accordance with the Arrhenius equation. The activation energy calculated based on temperature data is 45 kJ/mol.

Since the equilibrium during H_2SiF_6 saturation does not appear to change in this temperature range, saturation could also be expected to proceed faster at 35°C, resulting in shorter processing times. However, since saturation could be done overnight, this was not considered necessary for investigation.

7.6 Problems with LPD

Very little variation in deposition rates should result from variation in growth solution composition and deposition temperature. Yet notable variations exist in deposition rates, even under identical deposition conditions. The reason for this is unclear, and reference samples should therefore always be used when deposited film thickness is critical.

A greater problem is liquid phase nucleation and subsequent precipitation of SiO_2 particles in the growth solution. This limits the maximum film thickness obtainable in a single deposition step to less than 100 nm. This result is in contradiction with the results reported by many other investigators. Momentary, substantial oversaturation caused by the addition of water was suspected as the reason for this, but preparation of the growth solution by route II did not resolve the problem. Thus the reason for it also remains unknown.

References

[1] Angell, J. B., Terry, S. C., Barth, P. W., Silicon micromechanical devices, *Sci. Am.* **248** (1983) No 4, 36–47.

[2] Petersen, K. E., Silicon as a mechanical material, *Proc. IEEE* **70** (1982) 420–457.

[3] Hess, D. W., Plasma-assisted oxidation, anodization, and nitridation of silicon, *IBM Journal of Research and Development* **43** (1999) No 1. *http://www.research.ibm.com/journal/rd/431/hess.html*

[4] Deal, B. E., Helms, C. R., Vapor phase wafer cleaning technology, in *Handbook of semiconductor wafer cleaning technology: science, technology, and applications*, Ed. W. Kern, Noyes publications, Westwood, 1993.

[5] Campbell, S. A., *The science and engineering of microelectronic fabrication*, Oxford University Press, New York, 1996, 536 p.

[6] Grovenor, C. R. M., *Microelectronic materials*, IOP Publishing Ltd, Bristol, 1989, 544 p.

[7] Kurihara, K., Iwadate, K., Namatsu, H., Nagase, M., Murase, K., Electron beam nanolithography with image reversal by ECR plasma oxidation, *Microelectron. Eng.* **27** (1995) 125–128.

[8] Pierson, H. O., *Handbook of chemical vapor deposition: Principles, technology and applications*, Noyes Publications, Westwood, 1992, 436 p.

[9] Sherman, A., *Chemical vapor deposition for microelectronics—Principles, technology, and applications*, Noyes Publications, New Jersey, 1987, 215 p.

[10] Graper, E. B., in *Handbook of thin film process technology*, Ed. D. A. Glocker and S. I. Shah, part A, IOP Publishing Ltd, Bristol 1995, p. A 1.2:12.

[11] Thomsen, S. M., High-silica fluosilicic acids: Specific reactions and the equilibrium with silica, *J. Am. Chem. Soc.* **74** (1952) 1690–1693.

[12] Nicoll, F. H., Low reflection films on glass by an improved chemical method, *RCA Review* **10** (1949) 440–447.

[13] Thomsen, S. M., Low-reflection films produced on glass in a liquid fluosilicic acid bat, *RCA Review* **12** (1951) 143–149.

[14] Nagayama, H., Honda, H., Kawahara, H., A new process for silica coating, *J. Electrochem. Soc.* **135** (1988) 2013–2016.

[15] Hishinuma, A., Goda, T., Kitaoka, M., Hayashi, S., Kawahara, H., Formation of silicon dioxide films in acidic solutions, *Appl. Surf. Sci.* **48–49** (1991) 405–408.

[16] Chanthamaly, P., Arakawa, T., Haneji, N., Silicon dioxide film with low dielectric constants using liquid-phase deposition, *Jpn. J. Appl. Phys.* **38** (1999) 5715–5719.

[17] Yeh, C.-F., Chen, C.-L., Lin, G.-H., The physicochemical properties and growth mechanism of oxide ($SiO_{2-x}F_x$) by liquid phase deposition with H_2O addition only, *J. Electrochem. Soc.* **141** (1994) 3177–3181.

[18] Yeh, C.-F., Lee, Y.-C., Wu, K.-H., Su, Y.-C., Lee, S.-C., Comprehensive investigation on fluorosilicate glass prepared by temperature-difference-based liquid-phase deposition, *J. Electrochem. Soc.* **147** (2000) 330–334.

[19] Chou, J.-S., Lee, S.-C., The initial growth mechanism of silicon oxide by liquid-phase deposition, *J. Electrochem. Soc.* **141** (1994) 3214–3218.

[20] Homma, T., Katoh, T., Yamada, Y., Yukinobu, M., A selective SiO_2 film-formation technology using liquid-phase deposition for fully planarized multilevel interconnections, *J. Electrochem. Soc.* **140** (1993) 2410–2414.

[21] Shih, P.-S., Chang, T.-C., Huang, T.-Y., Yeh, C.-F., Chang, C.-Y., Characterization and reliability of lightly-doped-drain polysilicon thin-film transistors with oxide sidewall spacer formed by one-step selective liquid phase deposition, *Jpn. J. Appl. Phys.* **39** (2000) 5758–5762.

[22] Kanba, K., Horiuchi, T., Homma, T., Murao, Y., Okumura, K., A 7 mask CMOS technology utilizing liquid phase selective oxide deposition, *Proceedings, 1991 IEDM* 637–640.

[23] Horiuchi, T., Kanba, K., Homma, T., Murao, Y., Okumura, K., A 7-mask CMOS process with selective oxide deposition, *IEEE Trans. Electron Devices* **40** (1993) 1455–1460.

[24] Yeh, C.-F., Liu, C.-H., Su, J.-L., Novel contact hole fabrication using selective liquid-phase deposition instead of reactive ion etching, *IEEE Electron Device Lett.* **20** (1999) 39–41.

[25] Shih, P.-S., Chang, C.-Y., Chang, T.-C., Huang, T.-Y., Peng, D.-Z., Yeh, C.-F., A novel lightly doped drain polysilicon thin-film transistor with oxide sidewall spacer formed by one-step selective liquid phase deposition, *IEEE Electron Device Lett.* **20** (1999) 421–423.

[26] Lee, M.-K., Yang, C.-N., Lin, C.-H., Conformal step coverage and trench filling of liquid phase oxide deposition, *Jpn. J. Appl. Phys.* **38** (1999) 5048–5049.

[27] Chen, M.-S., Chou, J.-S., Lee, S.-C., Planarization of amorphous silicon thin film transistors by liquid phase deposition of silicon dioxide, *IEEE Trans. Electron Devices* **42** (1995) 1918–1923.

[28] Huang, C. J., Houng, M. P., Wang, Y. H., Wang, H. H., Effect of a chemical modification on growth silicon dioxide films on gallium arsenide prepared by the liquid phase deposition method, *J. Appl. Phys.* **86** (1999) 7151–7155.

[29] Wanh, N.-F., Hound, M.-P., Wanh, Y.-H., Investigation of low-temperature deposition of silicon dioxide on indium phosphide by liquid phase deposition, *Jpn. J. Appl. Phys.* **38** (1999) 6071–6072.

[30] Kitaoka, M., Honda, H., Yoshida, H., Takigawa, A., Kawahara, H., Formation of SiO2 film on plastic substrate by liquid phase deposition method, *Proc. SPIE* **1519** (1991) 109–114.

[31] Chang, P.-H., Huang, C.-T., Shie, J.-S., On liquid-phase deposition of silicon dioxide by boric acid addition, *J. Electrochem. Soc.* **144** (1997) 1144–1149.

[32] Chou, J.-S., Lee, S.-C., Inproved process for liquid phase deposition of silicon dioxide, *Appl. Phys. Lett.* **64** (1994) 1971–1973.

[33] Homma, T., Murao, Y., Properties of liquid-phase-deposited SiO_2 films for interlayer dielectrics in ultralarge-scale integrated circuit multilevel interconnections, *Thin Solid Films* **249** (1994) 15–21.

[34] Yeh, C.-F., Lin, S.-S., Yang, T.-Z., Chen, C.-L., Yang, Y.-C., Performance and off-state current mechanisms of low-temperature processed polysilicon thin-film transistors with liquid phase deposited SiO_2 gate insulator, *IEEE Trans. Electron Devices* **41** (1994) 173–179.

[35] Yeh, C.-F., Lin, S.-S., Chen, C.-L., Yang, Y.-C., Novel technique for SiO_2 formed by liquid-phase deposition for low-temperature processed polysilicon TFT, *IEEE Electron Device Lett.* **14** (1993) 403–405.

[36] Huang, C.-T., Chang, P.-H., Shie, J.-S., Photoassisted liquid-phase deposition of silicon dioxide, *J. Electrochem. Soc.* **143** (1996) 2044–2048.

[37] Operating manual for Philips SD 2300 ellipsometer, PLASMOS GmbH, München, 1995, p. 8-4.

[38] Lee, M.-K., Lin, S.-Y., Shyr, J.-M., Characteristics of oxynitride prepared by liquid phase deposition, *J. Electrochem. Soc.* **148** (2001) F1–F4.

[39] Kawahara, H., Goda, T., Nagayama, H., Honda, H., Hishinuma, A., SiO_2 Film grown on glass in aqueous solution, *Proc. SPIE* **1128** (1989) 2–7.

[40] Lu, W.-S., Hwu, J.-G., Preparation of fluorinated gate oxides by liquid phase deposition following rapid thermal oxidation, *Appl. Phys. Lett.* **66** (1995) 3322–3324.

[41] Middleman, S., Hochberg, A. K., *Process engineering analysis in semiconductor device fabrication*, McGraw-Hill, New York, 1993, 774 p.

[42] Yeh, C.-F., Lee, Y.-C., Lee, S.-C., Reliability of fluorinated silicon oxide film prepared by temperature difference-based liquid phase deposition, *J. Electrochem. Soc.* **147** (2000) 4268–4272.

[43] Lee, K.-C., Hwu, J.-G., 17.3% Efficiency metal-oxide-semiconductor (MOS) solar cells with liquid-phase-deposited silicon dioxide, *IEEE Electron Device Lett.* **18** (1997) 565–567.

[44] Yeh, C.-F., Chen, T.-J., Jeng, J.-N., Effects of process temperature on polysilicon thin film transistors with liquid-phase deposited oxides as gate insulators, *J. Electrochem. Soc.* **144** (1997) 3645–3649.

[45] Yeh, J.-L., Lee, S.-C., Amorphous-silicon thin-film transistor with liquid phase deposition of silicon dioxide gate insulator, *IEEE Electron Device Lett.* **20** (1999) 138–139.

[46] Deki, S., Aoi, Y., Asaoka, Y., Kajinami, A., Mizuhata, M., Monitoring the growth of titanium oxide thin films by the liquid-phase deposition method with a quartz crystal microbalance, *J. Mater. Chem.* **7** (1997) 733–736.

[47] Chung, J., Jeng, M.-C., Moon, J. E., Wu, A. T., Chan, T. Y., Ko, P. K., Hu, C., Deep-submicrometer MOS device fabrication using a photoresist-ashing technique, *IEEE Electron Device Lett.* **9** (1988) 186–188.

[48] Asano, K., Choi, Y.-K., King, T.-J., Hu, C., Patterning sub-30-nm MOSFET gate with I-line lithography, *IEEE Trans. Electron Devices* **48** (2001) 1004–1006.

[49] Niskanen, A. J., Franssila, S., Submicron image reversal by liquid phase deposition of oxide, *Microelectron. Eng.*, **57–58** (2001) 629–632.

Appendix A

Additional experimental data

The data presented in Tables A.1–A.7 was measured by ellipsometer at multiple points on the substrate surface. The average (AVG) and standard deviation (STDEV) of thickness and refractive index are presented. In Tables A.9 and A.10 the voltage ramping rate was 0.77 V/sec.

Table A.1: Effect of deposition temperature. 100 ml 25% H_2SiF_6, 16 ml H_3BO_3, 109 ml H_2O. Temperature increased between depositions.

Temp.	Time	Thickness (Å)		Refractive index	
(°C)	(min)	AVG	STDEV	AVG	STDEV
25	60	141.02	3.64	1.3703	0.0179
30	60	188.88	1.62	1.4083	0.0081
35	60	254.86	0.69	1.4201	0.0018
40	60	335.83	2.50	1.4192	0.0045

Table A.2: Effect of boric acid addition. 100 ml 25% H_2SiF_6, 100 ml H_2O, 35°C deposition temperature. H_3BO_3 added between depositions.

H_3BO_3 add.	Time	Thickness (Å)		Refractive index	
(ml)	(min)	AVG	STDEV	AVG	STDEV
0	60	85.96	7.29	1.4460	0.0834
5	60	129.41	1.21	1.4035	0.0077
10	60	176.56	2.05	1.4178	0.0096
20	60	302.90	0.61	1.4252	0.0022
40	60	627.17	2.38	1.4212	0.0019

Table A.3: Effect of water addition No 1. 100 ml 25% H_2SiF_6, 50 ml H_2O, 10 ml H_3BO_3, 25°C deposition temperature. 50 ml H_2O and 3.3 ml H_3BO_3 added between depositions.

H_2O add.	Time	Thickness (Å)		Refractive index	
(ml)	(min)	AVG	STDEV	AVG	STDEV
50	83	214.77	1.58	1.4172	0.0050
100	60	220.63	0.74	1.4214	0.0030
150	69	265.21	0.40	1.4248	0.0011
200	60	215.48	0.51	1.4215	0.0020
250	60	197.78	1.21	1.4062	0.0051

Table A.4: Effect of water addition No 2. 100 ml 25% H_2SiF_6, 50 ml H_2O, 5 ml H_3BO_3, 35°C deposition temperature. 50 ml H_2O and 1.7 ml H_3BO_3 added between depositions.

H_2O add.	Time	Thickness (Å)		Refractive index	
(ml)	(min)	AVG	STDEV	AVG	STDEV
50	60	92.57	1.64	1.3854	0.0138
100	60	152.59	0.90	1.4162	0.0047
150	55	156.23	1.44	1.4020	0.0070
200	55	149.81	1.37	1.4144	0.0077
250	55	137.10	1.54	1.4139	0.0084
300	65	146.88	0.46	1.4017	0.0022

Table A.5: Effect of water addition No 3. 100 ml 25% H_2SiF_6, 50 ml H_2O, 20 ml H_3BO_3, 35°C deposition temperature. 50 ml H_2O and 6.7 ml H_3BO_3 added between depositions.

H_2O add.	Time	Thickness (Å)		Refractive index	
(ml)	(min)	AVG	STDEV	AVG	STDEV
50	60	307.19	0.55	1.4236	0.0011
100	60	407.76	0.59	1.4287	0.0011
150	60	410.51	0.89	1.4222	0.0007
200	60	408.36	4.64	1.3850	0.0058
250	60	516.53	46.11	1.2552	0.0216

Table A.6: Effect of water addition No 4. 100 ml 25% H_2SiF_6, 150 ml H_2O, 33.3 ml H_3BO_3, 35°C deposition temperature. 50 ml $H_2O$and 6.7 ml H_3BO_3 added between depositions.

H_2O add.	Time	Thickness (Å)		Refractive index	
(ml)	(min)	AVG	STDEV	AVG	STDEV
150	60	378.27	0.91	1.4349	0.0022
200	60	384.12	2.58	1.4051	0.0029
250	60	436.77	25.38	1.2962	0.0179
300	60	836.54	96.58	1.1544	0.0097

Table A.7: Effect of water addition No 5. 100 ml 25% H_2SiF_6, 50 ml H_2O, 15 ml H_3BO_3, 35°C deposition temperature. 50 ml H_2O and 5 ml H_3BO_3 added between depositions.

H_2O add.	Time	Thickness (Å)		Refractive index	
(ml)	(min)	AVG	STDEV	AVG	STDEV
50	60	182.09	0.93	1.4359	0.0039
100	60	267.78	0.42	1.4333	0.0016
150	70	342.08	1.13	1.4326	0.0030
200	60	278.85	0.67	1.4295	0.0018
250	59	256.35	1.47	1.4180	0.0035
300	49	202.20	6.33	1.3814	0.0149

Table A.8: Uniformity of deposition across whole wafers in batch processing. 150 ml 25% H_2SiF_6, 225 ml H_2O, 25 ml H_3BO_3, 35°C deposition temperature, 63 minutes deposition time. Wafers face down.

Deposited oxide thickness (Å)						
Top wafer:						
		351.58	351.80	351.40		
	351.52	349.92	350.84	349.73	348.73	
349.53	349.96	349.68	350.00	351.21	351.15	349.75
348.07	348.24	349.36	349.14	348.70	346.06	344.77
346.27	347.65	348.57	348.35	348.60	346.97	345.93
	347.41	346.83	348.00	349.40	347.81	
		346.86	347.06	351.75		
Bottom wafer:						
		353.74	354.55	352.26		
	352.60	353.54	353.97	353.33	351.29	
352.80	353.25	353.79	354.46	353.04	352.17	348.94
352.37	352.49	353.00	353.80	353.27	351.67	350.50
352.66	352.24	352.75	352.95	352.86	351.98	351.09
	352.41	353.72	353.21	352.64	352.30	
		353.19	353.12	352.46		

Table A.9: Measured breakdown voltages in 500×500 µm MOS-capacitors with 72 nm LPD SiO_2 dielectrics

V_{BD} (volts)					
9.0	31.0	35.5	29.0	35.5	31.0
11.0	31.5	8.0	9.5	24.0	40.5
45.0	29.5	31.0	18.0	10.0	21.0
26.0	35.0	35.5	11.5	29.0	27.0
32.0	34.5	33.0	27.5	29.0	34.5

Table A.10: Measured breakdown voltages in 100×100 µm MOS-capacitors with 72 nm LPD SiO_2 dielectrics

V_{BD} (volts)					
22.5	9.5	17.0	27.0	20.0	25.0
34.0	9.0	32.5	29.0	30.5	27.5
29.5	33.0	22.5	14.5	29.0	30.5
13.0	21.5	22.0	24.0	11.5	11.0
31.0	21.5	25.0	25.0	17.5	25.0

Appendix B

Oxygen plasma ashing

AZ 5214E photoresist was spun at 5000 revolutions per minute for 35 seconds and prebaked 20 minutes at 90°C. Photoresist patterns were made with an etching test mask containing various test structures such as lines and dots down to 1 µm line width in both light field and dark field. After exposure and development the photoresist was postbaked for 30 minutes at 120°C. The photoresist film thickness, measured by reflectometer, was 1.41 µm.

The photoresist patterns were thinned in oxygen plasma at various power levels at 600 mTorr (80 Pa) pressure and 86 sccm O_2 flow rate. The thicknesses were measured by reflectometer. The results are presented in Table B.1.

A slightly higher etch rate is observed for etch times of 15 minutes than for 30 minutes, indicating slight hardening of the resist during etching and no thermal runaway in the reactor. Little or no effect on resist thickness uniformity or refractive index was observed. Fig. B.1 presents etch rates measured for 30 minute etch times at various RF power levels. SEM study of photoresist line cross-sections indicated nearly isotropic etching, only slightly faster in the vertical than in the lateral direction.

To demonstrate image reversal by LPD on the deep sub-micron scale, thinned samples were made by etching 30 minutes at 400 W on one sample and 15 minutes at 500 W on another. Several ultimately thin photoresist lines were found on both samples.

Table B.1: Photoresist etch rate at various RF power levels

Power (W)	Time (min)	Etch rate (nm/min)
150	15	13.1
150	30	9.8
250	30	14.5
400	30	21.1
500	15	24.5
500	30	27.0

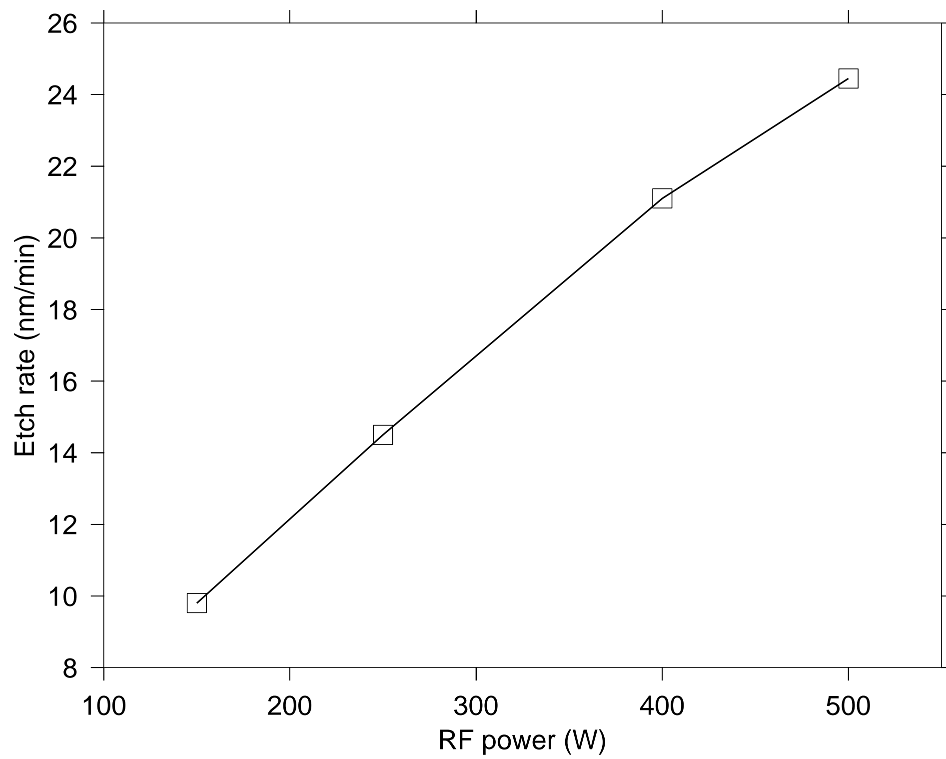

Figure B.1: Photoresist etch rate versus oxygen plasma RF power